SKB

TECHNICAL REPORT 90-43

GMM – A general microstructural model for qualitative and quantitative studies of smectite clays

Roland Pusch, Ola Karnland, Harald Hökmark
Clay Technology AB, Lund

December 1990

SVENSK KÄRNBRÄNSLEHANTERING AB
SWEDISH NUCLEAR FUEL AND WASTE MANAGEMENT CO
BOX 5864 S-102 48 STOCKHOLM
TEL 08-665 28 00 TELEX 13108 SKB S
TELEFAX 08-661 57 19

GMM - A GENERAL MICROSTRUCTURAL MODEL FOR QUALITATIVE AND QUANTITATIVE STUDIES OF SMECTITE CLAYS

Roland Pusch, Ola Karnland, Harald Hökmark

Clay Technology AB, Lund

December 1990

GMM

A General Microstructural Model for Qualitative and Quantitative Studies of Smectite Clays

December 1990

Roland Pusch
Ola Karnland
Harald Hökmark

Clay Technology AB
IDEON, 223 70 Lund

LIST OF CONTENTS

SUMMARY

A few years ago an attempt was made to accomodate a number of basic ideas on the fabric and inter-particle forces that are assumed to be valid in montmorillonite clay in an integrated micro-structural model and this resulted in an SKB report on "Outlines of models of water and gas flow through smectite clay buffers". This model gave reasonable agreement between predicted hydraulic conductivity values and actually recorded ones for room temperature and porewater that is poor in electrolytes. The model also contributed to the understanding of mechanisms involved in the development of swelling pressures and gas percolation. A major feature of the model, which concerned clay formed from bentonite granules being hydrated by taking up water from the surroundings, was that the basic microstructural units are stacks of smectite flakes with interlamellar water that has different properties than bulk water.

The present report describes an improved model that also accounts for effects generated by salt porewater and heating, and that provides a basis for both quantitative determination of transport capacities in a more general way, and also for analysis and prediction of rheological behavior in bulk. It has been understood very early by investigators in this scientific field that full understanding of the physical state of porewater is asked for in order to make it possible to develop models for clay particle interaction. In particular, a deep insight in the nature of the interlamellar water and of the hydration mechanisms leading to an equilibrium state between the two types of water, and of force-fields in matured smectite clay, requires very qualified multi-discipline research and attempts have

been made by the senior author to initiate and coordinate such work in the last 30 years. Despite this effort it has not been possible to get an unanimous understanding of these things but a number of major features have become more clear through the work that we have been able to carry out in the current SKB research work. Thus, NMR studies and precision measurements of the density of porewater as well as comprehensive electron microscopy and rheological testing in combination with application of stochastical mechanics, have led to the hypothetical microstructural model - the GMM - presented in this report.

It is self-evident that further improvements of the model are possible and they are expected to be required when using the model in practice, especially respecting functions that have not yet been tested.

1 INTRODUCTION

The use of smectite clays for isolation of radioactive waste in rock means that it will be exposed to changes in groundwater composition and to heat which will combine to alter the mineralogy and the physical properties of the clays. The mineralogical degradation, being insignificant at moderate temperatures and very slow uptake of potassium but quick and significant if the opposite conditions prevail, will not be discussed in the present report, which deals with mechanisms that control water and gas flow and ion diffusion, and the rheological behavior. The key parameter is the microstructural constitution of the clays, on which the report is focussed.

2 BASIC CONCEPTS

2.1 Bentonite material

We will take commercial bentonites in powdered or granular form as a basis of our presentation since they are commonly used for preparation of bentonite blocks to surround canisters or to plug drilled or blasted excavations. Good raw material which should have montmorillonite as major clay mineral*, is often saturated with calcium that is replaced by sodium through a simple conditioning process. Through this some minor amount of calcite is formed and this mineral, as well as minor amounts of quartz and cristobalite, feldspars, mica, and heavy minerals like pyrite, are also natural constituents. Usually, some amorphous aluminous silicates, yielding slight cementation is present as well. The smectite content hardly ever exceeds 80 %.

---

* Saponite, a Mg-rich variety, may be equally good or even superior to montmorillonite

2.2 Smectite/water/electrolyte systems

2.2.1 *Crystal lattice*

The exact nature of the montmorillonite lattice is not known and different views prevail. At present there are reasons to believe that two crystal structure types exist depending on temperature and type of interlamellar cation; the conventional Hofmann/Endell/Wilm (HEW) model for higher temperatures than 100 - 130°C and when other cations than Li or Na are adsorbed, and a low-temperature version - with Li or Na in interlamellar positions - that is of the type proposed by Edelman/Favejee (EF), i.e. with a certain fraction of the silica tetrahedrons inverted as indicated in Fig.1 (1). Their apices are hydroxyls forming hydrogen bonds with water molecules in the interlamellar space.

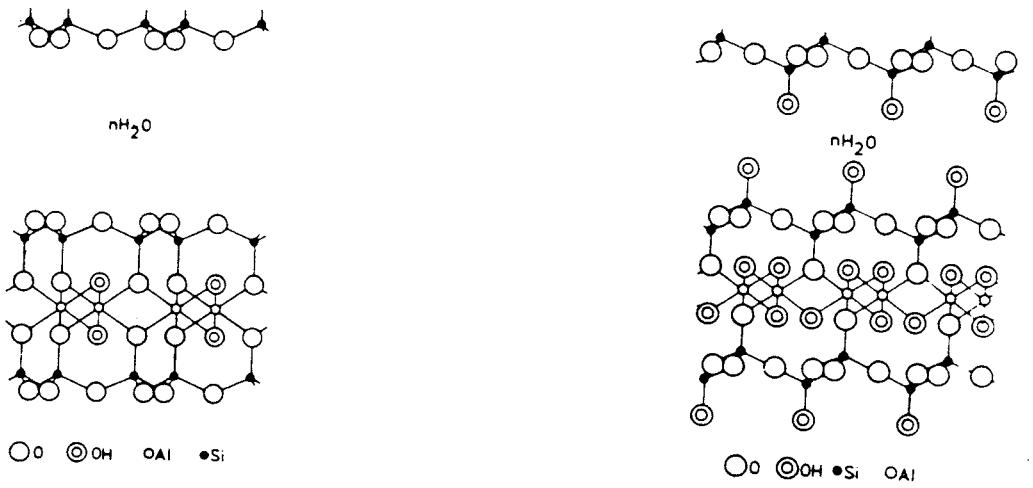

Fig.1 Montmorillonite crystal structure.
Left: HEW "high temperature form"
Right: EF "low temperature form" with Li or Na as adsorbed cation

2.2.2 *Hydrated crystal structure*

Applying the conventional Hofman/Endell/Wilm (HEW)-concept of the montmorillonite strcuture, the siloxane surfaces exposed in the interlamellar space have functional groups in the form of ditrigonal cavities which create relatively unstable water complexes in the absence of lattice substitution, and rather stable complexes with both cations and water molecules when there are lattice substitutions in the octahedral sheet (2). In beidellite, where there is isomorphic substitution of 25 % of the tetrahedral Si^{4+} by Al^{3+}, the charge is strongly localized to the three surface oxygens of the tetrahedron and much stronger complexes with cations and water molecules are formed, as illustrated by the hydrate thicknesses in Table 1.

Table 1. Thickness in Å of dehydrated smectite crystals and of complete hydrate layers as evaluated from sharp X-ray diffraction peaks (3)

		0 hydrate	1st	2nd	3rd
Montmorillonite	Mg (001)	9.52	3.00	3.03	3.05
	Ca (001)	9.61	2.89	2.75	-
	Na (001)	9.62	3.03	3.23	3.48
	K (001)	10.08	2.42	3.73	-
Beidellite	Mg (001)	9.85	2.69	2.69	-
	Ca (001)	9.95	2.30	2.30	-
	Na (001)	9.82	2.15	2.15	-
	K (001)	10.08	2.54	-	-

The table illustrates the general belief that the interlamellar water forms hydrate layers of which there are two in Ca- and K-saturated montmorillonite while there are three in Na- and Mg-saturated mont-

morillonite. Beidellite appears to hold only two hydrates when saturated with Mg, Ca, and Na, while it has been shown to have only one hydrate layer on saturation with K. One concludes from these data that in sodium montmorillonite the first hydrate layer is thinner than the second, which is in turn thinner than the third, least strongly adsorbed hydrate layer. The hydrates in calcium and magnesium montmorillonite are more equally and much more strongly adsorbed. Beidellite appears to retain its water most strongly and the two hydrate layers that can be formed seem to be equally strongly bound. The fact that only one layer is formed in K-saturated beidellite actually suggests that this smectite is partly converted to hydrous mica (illite) on K-uptake.

2.2.3 *Organization and physical properties of interlamellar water*

2.2.3.1 General

The arrangement of water molecules in the interlamellar space is a matter of debate. Inner- and outer-sphere complexes can be formed in the interlamellar space of which the two-layer hydrate of Ca-montmorillonite is a familiar example of the last-mentioned type (Fig.2). In the case of monovalent exchangeable cations, it is commonly assumed that the interlamellar molecular arrangement of a one-layer hydrate is like the one showed in Fig.3, the water molecules forming a strained ice-like lattice around monovalent exchangeable cations with bonds both intermolecularly and with the ditrigonal cavities (2). The lateral position of the water molecules is strongly correlated with the oxygens of the siloxane surfaces by which both hydrogen bonds and van der Waals forces become operative. If isomorphic substitution in the tetrahedral sheet exists, the hydrogen bonding is believed to be very significant. No

general model for the arrangement of the water molecules that constitute the second and third hydrates has been proposed for the HEW structure.

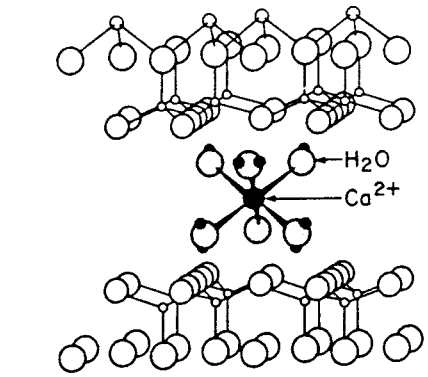

OUTER-SPHERE SURFACE COMPLEX:
$Ca(H_2O)_6^{2+}$ ON MONTMORILLONITE

Fig.2. Exploded view of surface complex of hydrated Ca ion in the interlamellar space (2)

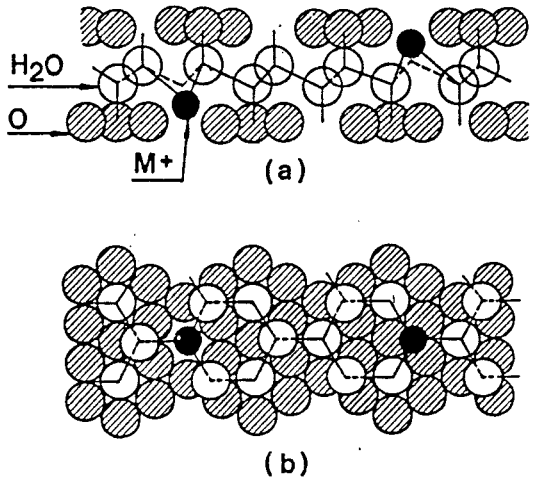

Fig.3. Structure of 1 hydrate interamellar layer in montmorillonite (After Mamy). The water molecules, which are shown grey,form an expanded ice lattice with 3 water molecules per 12 oxygen lattice atoms. Exchangeable cations are shown black in the upper plan view and in the section oriented perpendicularly (central picture). Lower picture shows influence of cation size on the water molcule arrangement

It is assumed that in the presence of bivalent exchangeable cations, the interlamellar region is organized more or less like a two-dimensional aqueous solution with relaxation properties like those of ice (2). Since the location of the charge deficiencies is not regular, it is logical to believe that the ordering of the water molecules is less good than in the case of small, monovalent cations.

An important fact is that the interlamellar spacing is not significantly altered even by large changes in the electrolyte content (Table 2). This is explained by the fact that the number of interlamellar cations is determined by the charge deficiency, which is a material property that does not depend on the overall electrolyte content.

Table 2. XRD (001) peaks in Å of Na montmorillonite (MX-80) under air-dry and water saturated conditions and with different salt contents

NaCl, ppm	0	5000	10000	20000	50000
Air.dry (RH 50 %)	14.5	12.55	12.54	12.60	12.60
Wet, (RH 100 %)	19.0	18.96	18.66	18.80	18.40

The values for air-dry material with salt of all the investigated concentrations agree almost exactly with that of Na Wyoming montmorillonite with 1 hydrate layer in Table 1. The higher value for non-salt montmorillonite is explained by non-parallel arrangement of the stacks. It represents integrated peaks of aligned as well as non-parallel flake assemblies. The (001)-value of the wet materials, i.e. 18.4 to about 19 Å,correspond fairly well to that of 3 hydrates in Table 1.

The alternative structural EF model of montmorillonite, which was refined by Forslind (1) to encompass several hydrates, also implies that the water molecules form a strained ice-like lattice. However, they are assumed to grow directly on interlamellar basal surfaces that are characterized by apical acid OH:s of a fraction of the silica/oxygen tetrahedrons. This arrangement, which is shown schematically in Table 3, yields theoretical (001) spacings that are not in very good agreement with those of Table 1 and it is also seen that Forslind's numbering of hydrates is not equivalent to that of the table. This may be explained by the fact that recorded XRD data represent averages of stable states with varying numbers of hydrate layers, mixed with unstable states.

Hydrogen bonds were assumed by Forslind to be responsible for the strength of the water lattice, weaker ones prevailing in the unstable states and strong ones in the stable layers, particularly when adjacent flakes are directly coupled through interacting apical OH groups. For pyrophyllite, which lacks lattice charge but is otherwise similar to montmorillonite, the hydration energy is about two thirds of that of the first hydrate layer of Na montmorillonite but only one fourth of that of Ca montmorillonite (3). This supports Forslind's idea of hydrogen bonds established between basal planes and an interlamellar water lattice in Na montmorillonite, and strong direct hydration of Ca ions in Ca montmorillonite.

In Forslind's EF structure there are 8 hydroxyls per three unit cells of (001) planes, forming 4 H bonds with the water lattice (Fig.4). He concluded that the charge of the crystallite will attain a mean value of 2/3 of a charge unit, meaning that no lattice substitutions would be required to account for the exchange capacity, which can have the form of replace-

ment of two protons at maximum per three clay unit cells. Cation exchange of Na montmorillonite would then have a large impact on porewater pH, which is actually the case.

Table 3. Forslind's model for the formation of interlamellar hydrates in montmorillonite

	Schematic interlayer structure	H_2O molecules per unit cell	Basal spacing, Å	g H_2O/g clay	mM H_2O/g clay	Remarks
0	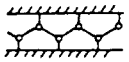	0	12.30	0; 0,084*	0; 4.667*	Unstable; no hydration; four OH groups per unit cell
1	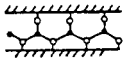	2.66	15.05	0.059	3.278	Unstable
2	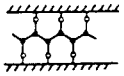	5.33	17.81	0.119	6.661	Stable monolayer
3	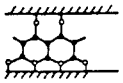	8.0	18.73	0.179	9.944	Unstable
4	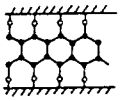	10.67	21.49	0.238	13.222	Stable; two layers
5	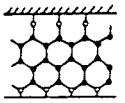	13.32	22.41	0.297	16.5	Unstable
6	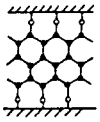	16.0	25.17	0.357	19.833	Stable; three layers

* At complete dehydroxylation.

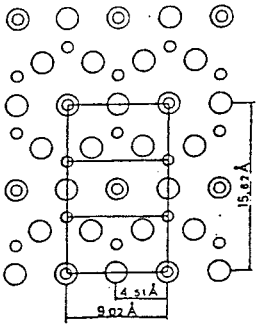

Fig.4 Forslind's interlamellar hydration pattern

2.2.3.2 Density of interlamellar water

The density of interlamellar water has been a matter of dispute for decades, the literature offering mean values ranging from 0.7 to 1.4 g/cm^3. Naturally, the organization of the water molecules is a determinant of the density of the water and it follows from the various possible hydration mechanisms and stages that the average density may well be in the range mentioned. A few years ago an attempt was made to determine the density by applying a very careful experimental procedure, i.e. dilatometry, and this study indicated a lower average density of interlamellar water than unity (about 0.9 g/cm^3) in the case of Na montmorillonite, in good agreement with reinterpreted data published by Low & Anderson (4). This was taken as a support of the idea of the interlamellar water forming a strained ice lattice in Na montmorillonite.

As inferred from Forslind's theory of montmorillonite hydration, interstitial "free" water molecules may well be present in the interlamellar space, especially in the "unstable" hydration stages, and this would mean that the porewater pressure may have an influence on both the stability of the interlamellar water lattice and the amount of water that can be brought into the interlamellar space. This has been investigated by applying backpressure to a water saturated clay sample while carefully measuring the change of volume of both samples and expelled or absorbed water in consolidation and swelling experiments.

The test arrangement is shown in Fig.5. Powdered MX-80 bentonite was placed in the oedometer for degassing at less than 0.1 kPa at 90^{o}C and subsequent saturation with deaired and deionized water after cooling. The sample was allowed to take up water for 1 month and was then heated to 90°C for 24 hours. The aim of the second heating was to ho-

mogenize the system and to create high internal water pressure for dissolving remaining air. The entire system of filters and tubings was also evacuated. The finally attained equilibrium state was established under a normal stress (swelling pressure) of 3 MPa giving a saturated density of approximately 1.95 g/cm^3.

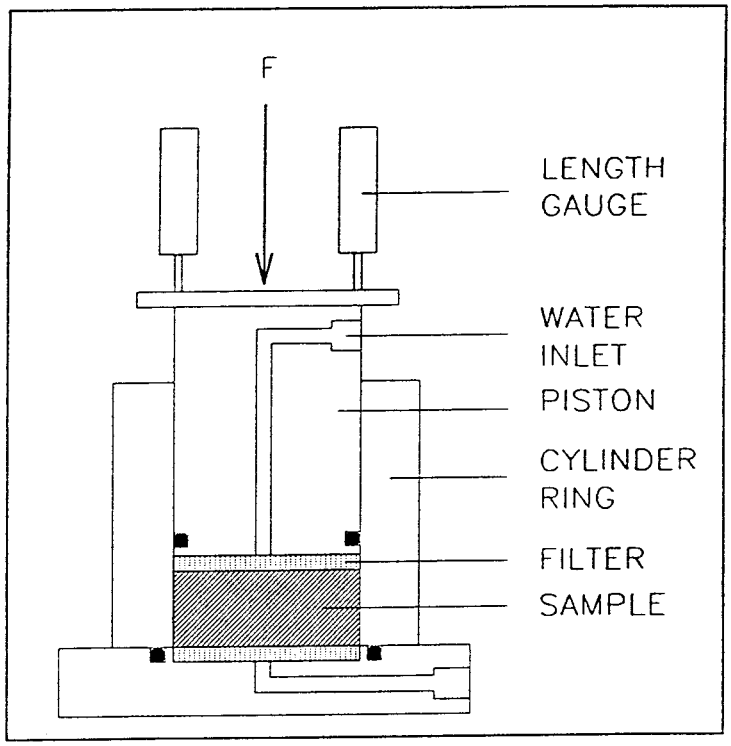

Fig.5 Schematic view of the test arrangement

Instantaneous disturbance of the system was imposed by either increasing the total pressure or increasing the porewater pressure according to the scheme in Fig.6. The main test cycle was conducted at a water backpressure of 250 kPa and additional tests at 800 kPa backpressure. The normal stress was varied between 600 and 5000 kPa corresponding to densities between 1.75 and 2.0 g/cm/^{3}. The effect of an increase in pore water pressure is similar to a decrease in normal stress, resulting in water uptake and expansion of the clay-water system. A typical plot of this process is shown in Fig.7.

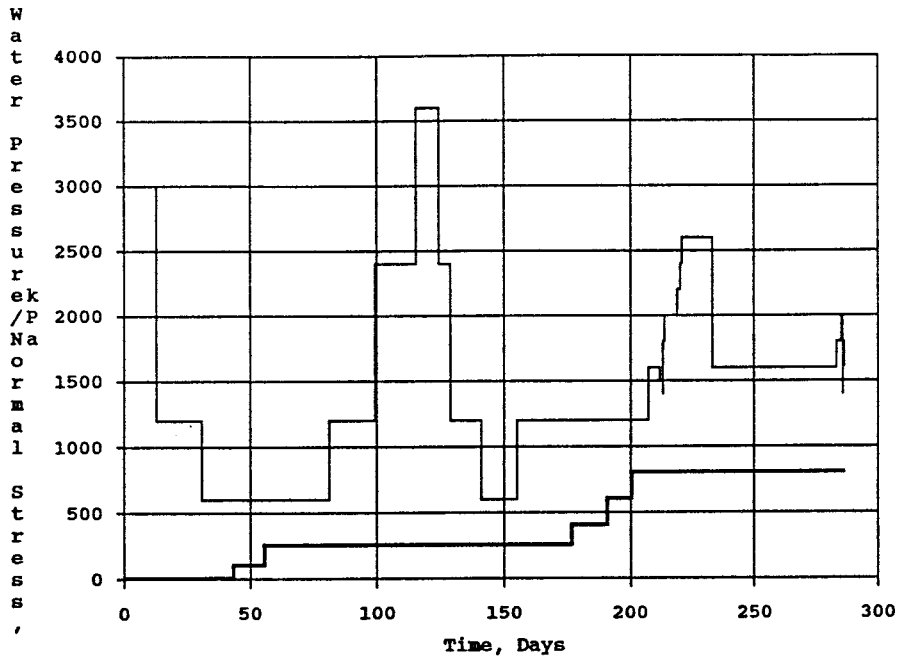

Fig.6 Scheme for evaluation of porewater density. Thin line shows normal stress, fat line the applied pore pressure

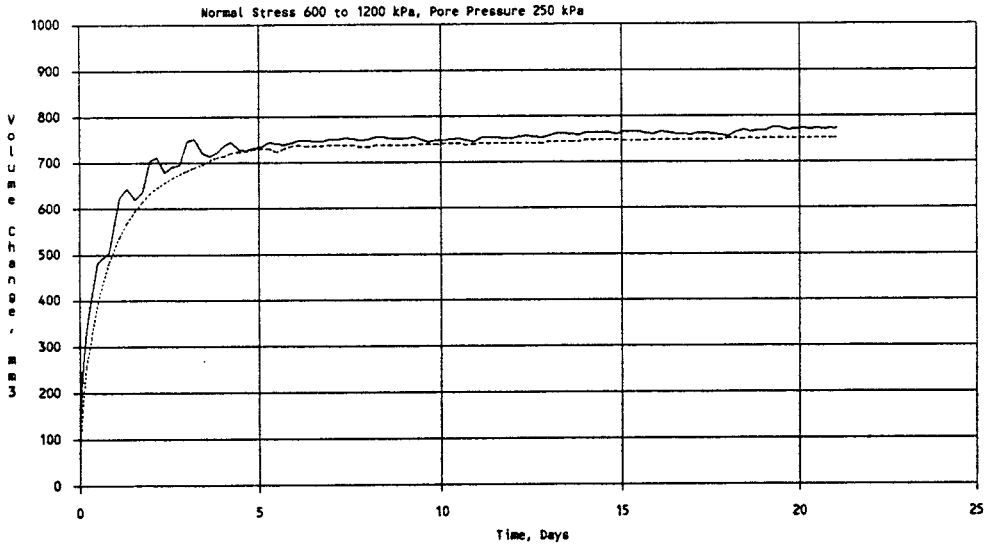

Fig.7 Recorded change in total volume (full line) and expelled water volume (dotted), resulting from an increase in stress from 600 to 1200 kPa, applying a water pressure of 250 kPa

The mean porewater density consistently turned out to be slightly higher than that of liquid water for the investigated clay densities, the maximum value being around 1.05 g/cm^3. The study shows that the porewater pressure affects the physical state of the water making the matter of the density of interlamellar water very complex.

The pore pressure was initially high at the onset of consolidation and dissipated in the course of water expulsion to the applied water pressure. As illustrated by Fig.7 unstable conditions with temporary drops in the ratio of the change in volume of the consolidating sample and of the expelled water appeared in the first few days but even after very long periods of time the volume of the expelled water exceeded the reduction of volume of the total sample. This led to the conclusion that the initial, big difference originated from a disturbance of the adsorbed water mass related to shear strain and to the porewater overpressure, and that water lattice restoration was achieved when much of the microstructural strain had ceased and the pore pressure had become sufficiently low.

A critical state was obviously reached when the pore water pressure was equal to the swelling pressure of the clay-water system. In the described test series, it resulted in an unstable state of equilibrium, which was recorded as intermittent flow of water into and out of the sample (Fig. 8). At this critical pore pressure partial water lattice breakdown took place with some interlamellar water supposedly leaving the interlamellar space and being converted to ordinary free porewater. This phenomenon is assumed to have started at random places in the sample and to have resulted in local pore pressure changes, forcing more interlamellar water to leave its position. This "chain

reaction" was compensated by the pressure-controlling device, the inertia of the system being responsible for the regular 10 minute pulses of flow in and out of the clay sample.

Two major conclusions were drawn from the study, the major one being that the density of the ordered interlamellar water in Na montmorillonite does not have a fixed value but ranges between about 1 and 1.05 g/cm^3 depending on the degree of ordering and presence of interstitial water molecules. A second outcome of the study is that the porewater pressure affects the interparticle force equilibrium in the sense that a porepressure that is equal to the swelling pressure creates unstable conditions. Although this does hardly have any significant practical effect it may have a bearing on the applicability of the effective stress concept.

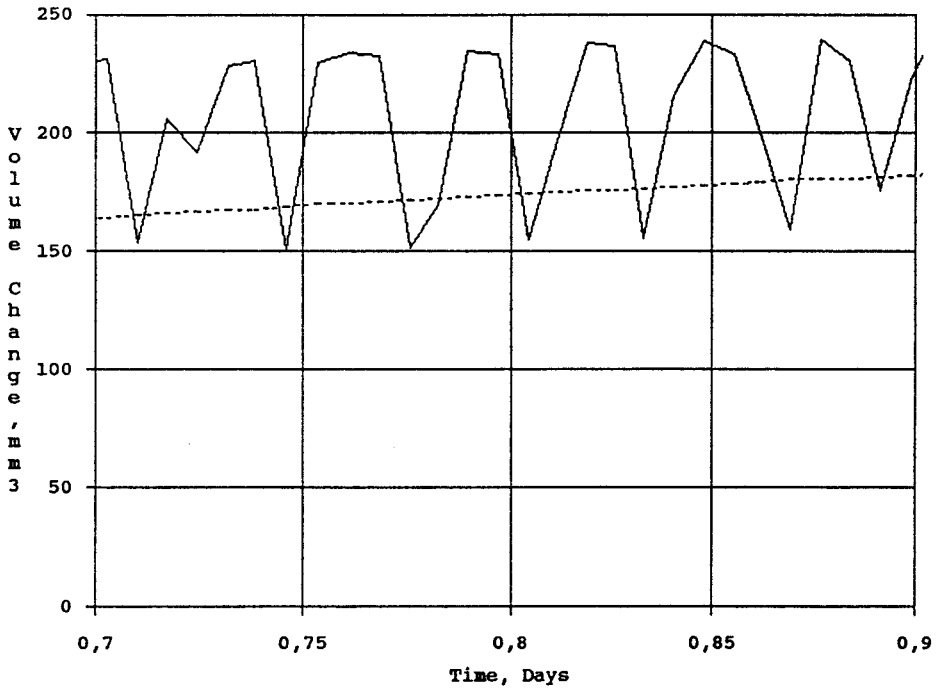

Fig.8 Pulse-type variation in volume changes of the sample and the expelled water. Applied water pressure 800 kPa, normal stress change from 1400 to 1800 kPa

The reason why numerous laboratory studies have yielded very low values of the density of smectite porewater seems to be that no backpressures were applied. This probably prevented formation of complete hydrates and yielded interlamellar water in the form of patches. Naturally, the application of backpressures also brings in interstitial water molecules that add to the interlamellar water mass and affect the intermolecular force fields.

2.2.3.3 Present physical model of interlamellar water

Practically all information referred to in the preceding text supports the belief that interlamellar water has a high degree of ordering but that it is of different origin in Na and Ca montmorillonite. As to the structuring of this water it is concluded that while the HEW model seems to be valid in principle for most types of interlamellar cations, there is still room to believe that such water can be organized in a fashion that is similar but not necessarily equal to Forslind's EF version if sodium is located in the interlamellar space. The main reasons for this are:

1. pH is strongly increased when exposing Na montmorillonite to electrolyte-free water. This is due to spontaneous release of exchangeable sodium that is replaced by protons probably through the formation of reactive hydroxyls exposed in the interlamellar space

2. The (001) spacing of Na montmorillonite is independent of the concentration of Na

in the porewater, i.e. the water molecule organization in the interlamellar space is not or only partly controlled by hydhydrated sodium ions

3. Diffusion of sodium takes place at such a rate and with such a capacity that Na ions cannot be significantly hydrated in the interlamellar space. Ordered hydrates are formed which are thought to be due to growth of interlamellar water lattices on the confining basal planes

4. Recent MAS/NMR studies support the assumption that inverted silica tetrahedrons with apical hydroxyls exist in montmorillonite (5)

From a practical point of view the most important feature of interlamellar water is that it forms an ordered medium in or through which interparticle forces are established and transferred. The organization of this medium is manifested by doublets in proton NMR spectra which disappear at temperatures exceeding room temperature by a few tens of centigrades, thereby indicating water lattice breakdown and increase in molecular mobility (6). Equally important is that part of the interlamellar water is in a relatively free state in the form of non-associated, interstitial molecules, meaning that the entire interlamellar water is a dynamic adsorption phase.

The force-fields operating on a microstructural scale in smectites will be discussed in detail later in the report.

2.3 Microstructural features

2.3.1 *"Internal" and "external" water*

Smectite clays appear to consist of interwoven systems of stacks of flakes separated by interlamellar ("internal") water. The system of stacks, often termed quasicrystals, contains voids with free, "external" water (Fig.9). The voids are interconnected to a certain extent, thereby forming passage-ways for water transport under hydraulic gradients and for anion migration. Anion transport through the stacks does not take place because of Donnan exclusion. The presence of interstitial water molecules in the interlamellar space means that the stacks are somewhat permeable but their contribution to the overall hydraulic conductivity is probably negligible.

Since silica surfaces in general are considered to be partly hydroxylated and thereby coated with 1-3 hydrate layers, it is probable that voids with an average diameter of up to 30 Å contain water that is largely immobilized, like the interlamellar water. It is quite obvious then that microstructural quantification is a requirement for the definition of the various amounts of water with different physical properties. This has been made by applying transmission electron microscopy using specimens first soaked with ethylene alcohol and then with plastic monomers, and by using high voltage electron microscopy for studying hydrating clay, and also by applying scanning electron microscopy. None of them yields perfectly undisturbed specimens but they all contribute to give a rather unanimous picture of how smectite flakes are organized both at high and low bulk densities.

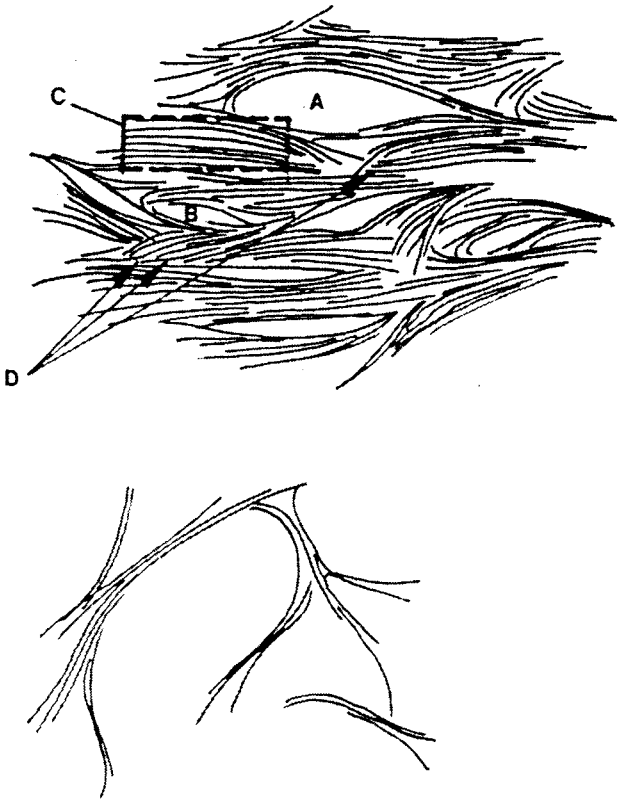

Fig.9 Microstructural features of smectite clays.
Upper: Dense clay with A) large and B) small void with "external" water, C) stack of flakes, D) Interface between stacks.
Lower: Expanded Na smectite clay gel with practically only external water

We will distinguish only between two major types of voids that hold water with very different properties: the interlamellar space and the voids between stacks of aligned flakes with equally oriented

crystal axes. The number of flakes is usually very small; there are reasons to believe that it is 3-5 in Na montmorillonite while it is 10-20 and occasionally more than that in Ca montmorillonite. Various types of microstructural investigations have led to the relationsship shown in Fig.10, which demonstrates that the volume of interlamellar water forms around 10 % of the total water volume in pure Na montmorillonite at a dry density of 0.35 g/cm^3 (1.22 g/cm^3 at water saturation) and more than 90 % at a dry density exceeding 1.60 g/cm^3 (2.0 g/cm^3 at water saturation). In Ca montmorillonite the corresponding percentages are almost the same but the content of internal water is appreciable smaller at intermediate densities.

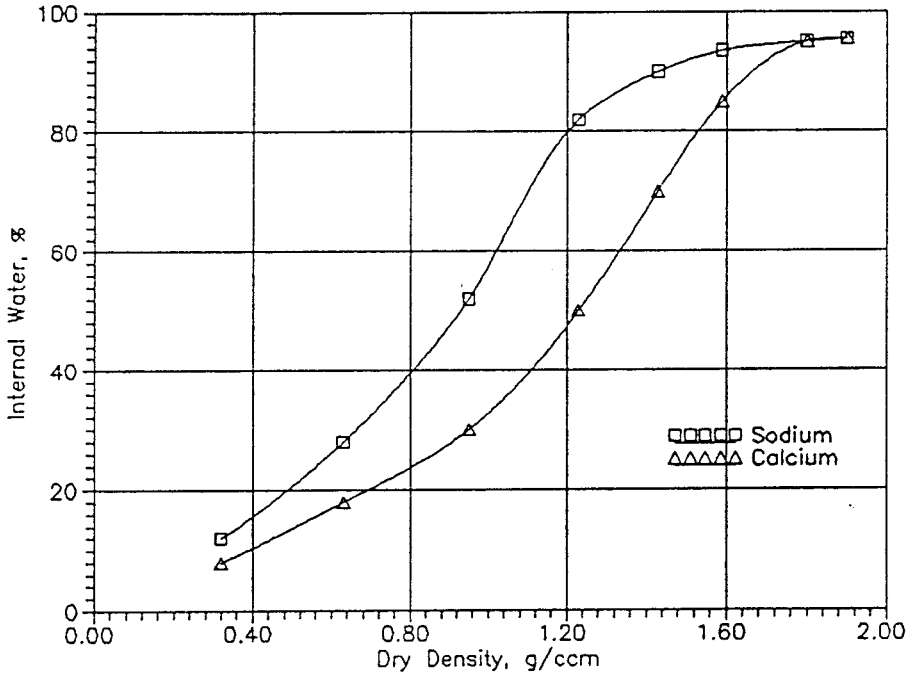

Fig.10 Theoretical relationship between dry bulk density and content of "internal" water expressed in percent of the total pore volume

2.3.2 Primary particles - stacks of flakes

Natural bentonite beds, formed from volcanish ash, are often consolidated under an appreciable overload that has produced alignment of the stacks of flakes that are characteristic primary structural units. This means that the powder or granulated material consists of grains with an inherited anisotropic structure (Fig.11). One can assume that the previously mentioned numbers of flakes in the stacks are still valid, i.e. that they consist of 3-5 flakes with equal orientation of the crystal axes when the smectite is in sodium form, and that the number averages at 10-20 when it is saturated with calcium.

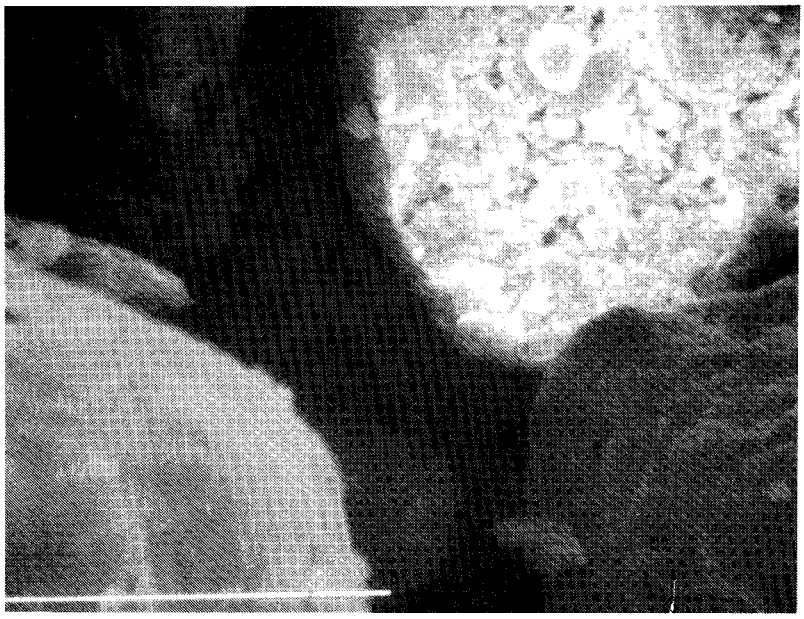

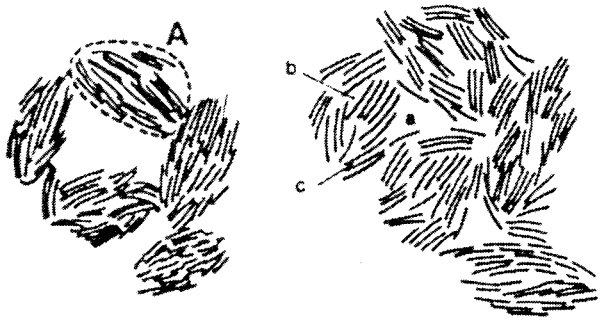

Fig.11 Bentonite granules (Scale 100 μm). Lower fig.: Granules (A) with non-swelled stacks (left), and expanded stacks. a and denote voids and c interlamellar space

The stacks remain as microstructural units on expansion and compression and operate as "particles" with both internal and external electric charge. The first-mentioned charge, which is due to lattice vacancies and substitutions, is balanced by cations adsorbed in the interlamellar space, while the other is neutralized by formation of electrical double-layers at the external stack surfaces. The significant difference in the number of flakes per stack, and hence of the number of contacts between stacks at a given bulk density, is of fundamental importance for the behavior of sodium- and calcium-saturated smectite clays.

2.3.3 *Interaction of minerals*

2.3.3.1 The force field in smectite clays

The study of the effect of backpressure demonstrates that the effect of water pressure is important and that the basic concept of *effective pressure* is not valid under all circumstances. We will consider some of the constituents that determine the shear strength and that combine to give the bulk swelling pressure of smectite clays although the matter is not yet fully understood. A major factor is naturally the interlamellar water, but we will also consider the interface between the stacks where electrical double-layers determine the interaction between the minerals and control the entire physical behavior of the clays at lower bulk densities. The very important matter of redistribution of "internal" and "external" water, which makes the development of stress equilibrium a very time-consuming process, will be touched on as well.

2.3.3.2 Interaction of stacks

The fact that water separates the flakes means that interaction between the mineral constituents largely takes place through water hydrates in smectite clay. The shear resistance of such clays is therefore a measure of the physical state of the "internal" water. Where stacks are closely located, forming more or less edge/face contacts it is assumed that there are also direct mineral/mineral contacts with strong bonds established in the surrounding of which electrical double-layers prevail (Fig.12). This suggests that the interparticle bonds vary from very strong ones, represented by primary valence bonds, to very weak hydrogen bonds. This matter will be considered later in the report.

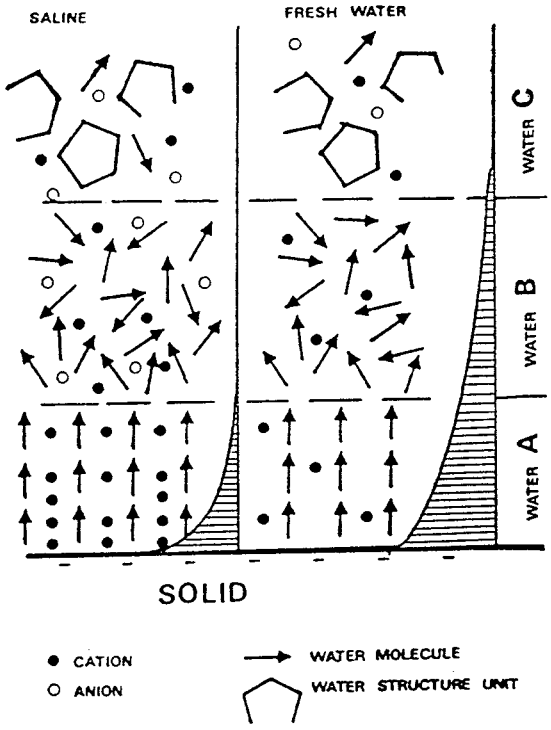

Fig.12 Schematic picture of electrical double-layers in saline and fresh water, respectively

Fig.12 makes use of Drost-Hansen's water structure model in which A is immobile vicinal water corresponding to the commonly assumed surface-associated water located inside the electrokinetic plane of shear, B water that is highly mobile under electrical potentials especially in fresh water, and C normally structured water (7). A is estimated to extend no more than about 10 Å from the external basal planes, while B may have an extension of a few tens of Å.

2.3.3.3 Electrical double-layers

While ordinary electrical double-layer theories account for both repulsive and attracting forces, they usually do not consider the influence of the water phase but the introduction of Drost-Hansen's water structure model may offer some help in understanding the mineral/water interaction. Thus, this theory nicely explains the dependence of salt concentration on the electro-osmotic flow capacity of clayey soils. Hence, water transportation through migration of hydrated cations, or through "drag" effects on water by migrating cations, is more effective in fresh than in salt water since cations dominate in the low-viscous B-zone at low salt concentration.

The repulsive forces exerted by interacting double-layers of neighboring stacks are counteracted by attraction caused by London/van der Waals forces and also by hydrogen bonds established between contacting A-zones at very small distances between the stacks. Applying electrical double-layer theories in the form proposed by Yong & Warkentin (8) gives fair agreement with actually recorded swelling pressures of both Na and Ca-saturated montmorillonite clays for a narrow dry density span, i.e. between 1.3 and 1.6g/cm^3 (1.8 to 2.0 g/cm^3 at water

saturation) but tends to yield much too low pressures at higher densities and too high pressures at lower densities as demonstrated by Fig.13. The model is developed for systems of parallel particles with overlapping diffuse layers of exchangeable cations and accounts for swelling by formation of a few surface-associated hydrate layers and further swelling resulting from osmotic pressure.

The reason for the too high values at low densities given by the model is that there is a deviation from the parallel particle concept, while the too low values at high densities are explained by underestimation of the hydration power of neighboring surfaces. Historically, Derjaguin and Obuchev showed already before the second world war that diffusive electrical double-layers produce a "disjoining" pressure that is only a fraction of the actual repulsive forces (10). Frenkel concluded from experiments with phyllosilicate minerals that mass forces and entropy effects are responsible for the major repulsion at small interparticle distances and found that colloidal particles remain attached to each other by extremely thin films of water if there is an ordering influence of the solids (11). Similar views are held by Low in a number of papers published in the last 30 years (cf. 12,13).

Common physical models covering interaction of electrical double-layers, surface-associated water, and attractive forces like the Yong/Warkentin and the Derjaguin/Landau/Verwey/Overbeek (DLVO) theories, which imply that interaction between plane surfaces of solids separated by water takes place through electrostatic repulsive forces and attractive mass forces, have to be equipped with an additional repulsive term to account for the very significant increase in repulsion that takes place as the solids are pressed together to distances on the

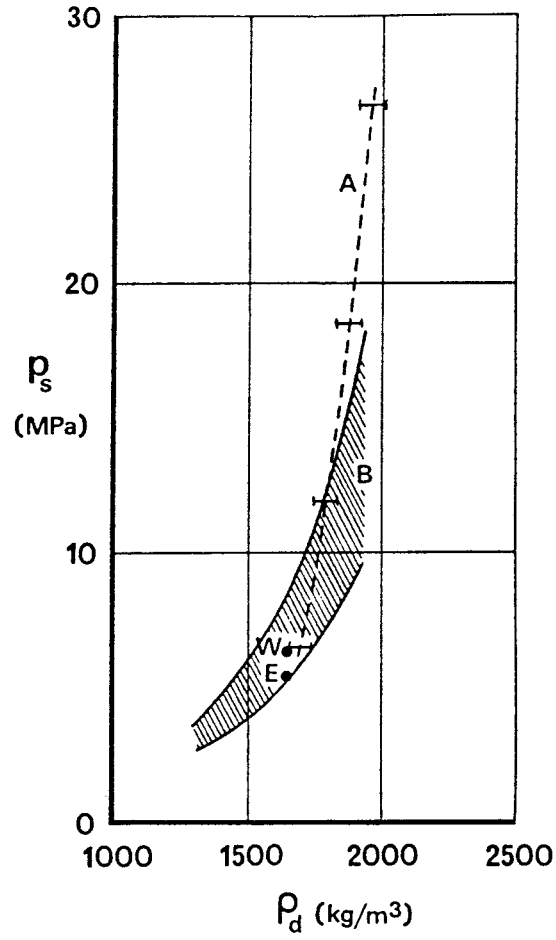

Fig.13 Swelling pressure versus dry density. Hatched area B represents theoretical net repulsive pressure with upper boundary for $3x10^{-3}$ M NaCl and lower for $>3x10^{-2}$ M NaCl (9). Recent data give higher pressures at low densities for Na montmorillonite

Broken curve A shows recorded pressures for Na and Ca montmorillonite clay. E and W represent commercial Ca and Na bentonites, respectively

order of 10 Å. Both mica grains and montmorillonite stacks give example of this, the probable explanation being the presence of steric, stabilizing wat-

er structures, as suggested by several authors (14,15).

2.3.4 *Nature of bonds*

2.3.4.1 General

It is concluded from the preceding text that although there are probably some direct mineral/mineral contacts in montmorillonite clays as in clays with hydrous mica or kaolinite as major mineral, water molecules appear to form most of the bonds that give smectite clays their expandability and shear resistance. More detailed information on this matter can be obtained by considering proton NMR data and rheological data.

2.3.4.2 Interlamellar water

XRD data and studies of the heat of immersion suggest that there is a considerable difference in strength of the respective hydrates of the interlamellar water network. Neither of these techniques give unanimous information on this issue due to microstructural effects and interaction of hydration of external and interlamellar space, but the authors' model of the respective amounts of external and internal water can be used in combination with proton NMR data for solving the problem. For this purpose Woessner's exploratory investigation into the range of surface effect on water molecule rotation will be used (16), while NMR data are extracted from (17).

Woessner's evaluation of the NMR parameter T_1 was based on the assumption that the number of interlamellar "surface-sorbed" water molecules is directly proportional to the inverse of the water

content, which is not correct for water saturated smectite clays. Using the diagram in Fig.10 and taking the fraction of interlamellar water f_s to be $V_i/(V_i+V_e)$, where V_i and V_e are the interlamellar or internal water and the external water volumes, respectively, and defining f_b as the fraction of bulk water, i.e. ($f_s+f_b=1$), and also assuming that we have:

$$1/T_1=f_b/T_{1b} + f_s/T_{1s} \quad (1)$$

where T_1 is the wheighted average for T_1 for all the aqueous protons, we arrive at the relationship:

$$1/T_1=1T_{1b} + f_s(1/T_{1s} - 1/T_{1b}) \quad (2)$$

Assuming that the conditions are such that one can apply this expression also for the proton relaxation time T_2, which requires proportionality of the relaxation times as has also been demonstrated experimentally (17), we have:

$$1/T_2=1/T_{2b} + f_s(1/T_{2s} - 1/T_{2b}) \quad (3)$$

This offers a way of distinguishing between the physical state of internal and external water at different water contents but it is clear that since T_2 is fundamentally complex because of the continuous exchange of surface-associated and non-associated water molecules the exchange of hydrogen nuclei between water molecules, the use of Eq.3 is not expected to yield an exact answer. The influence of paramagnetic effects that was earlier considered as a serious problem does not appear to be critical (17).

Carlsson's recordings of T_2 were made by use of Na montmorillonite clay (MX-80 bentonite) samples saturated with water with different salt contents and investigated at different temperatures. Fig.14

shows T_2 as a function of temperature and total water content and applying the data for room temperature, taking T_{2b} to be very much higher than T_{2s}, Eq.3 yields the result that T_{2s}, i.e. the relaxation time of the interlamellar water, is extremely short and not very much dependent of the total water content (Table 3). This means that the interlamellar water, i.e. 1-2 hydrates for a total water content w=20 %, 2-3 hydrates for w=40 %, and 3 hydrates for w>50 %, is highly ordered and that there is no very significant difference in adsorption strength of the various hydrates. Still, it is clear that the first hydrate is more strongly adsorbed than the second, which is in turn more strongly adsorbed than the third one.

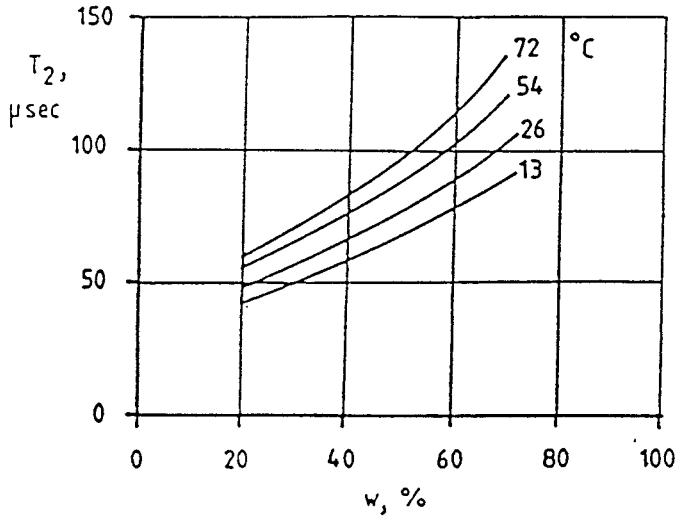

Fig.14 Recorded T_2-values for MX-80 clay (17)

Table 4. T_{2s} evaluated from Carlsson's data. MX-80 Na montmorillonite clay with distilled water at room temperature

Total water content %	T_{2s} μs
25	40
40	44
70	45
100	50

The diagram in Fig.14 shows that temperature has a significant influence on the average proton relaxation time. Thus, one finds that T_2 is almost 50 % higher at 72°C than at room temperature. Woessner's data on sodium saponite and beidellite shows about twice as large increase in relaxation time, which suggests that the less strong increase in Carlsson's experiments is due to a heat-induced reduction in the number of hydrate layers.

Carlsson's experiments with different salt solutions indicate that the average proton relaxation time for potassium, calcium and strontium is shorter than for sodium (Fig.15). Considering first sodium montmorillonite it is concluded that the addition of salt to about 5000 ppm concentration did not cause any change of the average T_2-value 130 μs that was recorded for a mixture of clay and distilled water with 100 % water content. Hence, the number of hydrates was not affected by the addition of NaCl, which is in agreement with the observation from XRD tests that the basal spacing is not altered by adding sodium chloride.

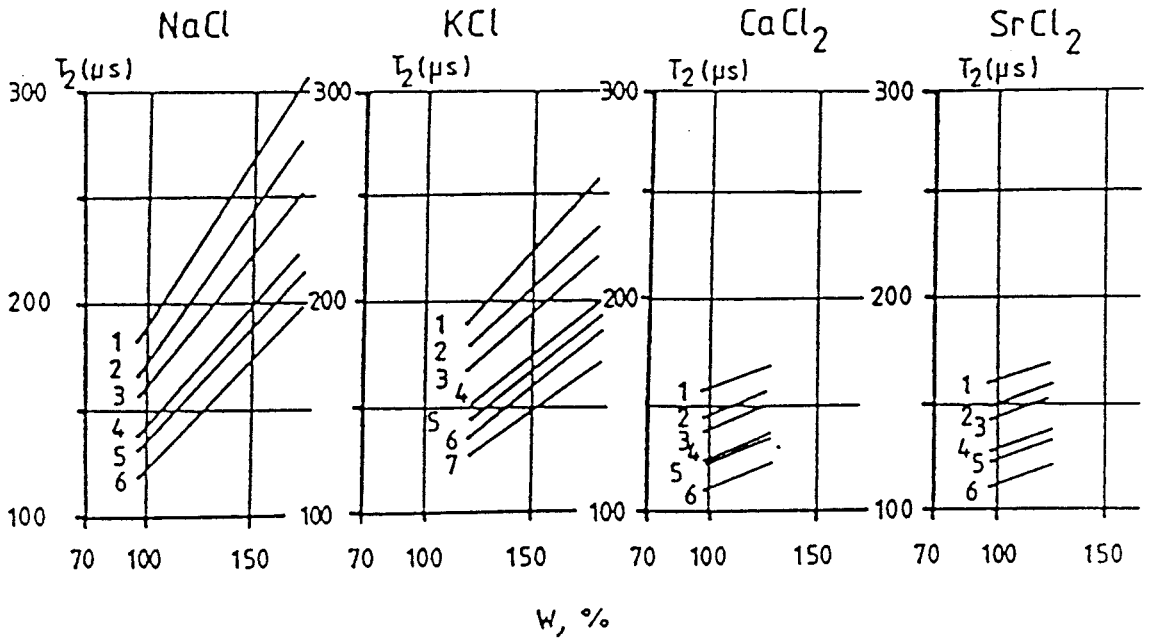

Fig.15 Generalized T_2-values evaluated from measurements of MX-80 clay saturated with 0.175 M solutions of NaCl, KCl, $CaCl_2$ and $SrCl_2$ (17). Figures refer to temperatures 1: T=82°C, 2: T=67°C, 3: T=57°C, 4: T=41°C, 5: T=33°C, 6: T=24°C, 7: T=17°C

As to the Ca clay, Carlsson's study only concerned samples with a water content of 90 to about 125 %, i.e. close to the Atterberg liquid limit, for which one can estimate f_s to be about 25 %. Putting this value into Eq.3 one finds T_{2s} for room temperature to be smaller than 30 μs, which is significantly lower than for sodium. This verifies that inter-lamellar water is more strongly bound in inter-lamellar positions than in the sodium case. In this respect strontium clay behaves in a similar fashion as calcium, while potassium represents an intermediate case.

The NMR proton study does not contradict Forslind's idea that hydrogen bonds are responsible for the establishment of interlamellar hydrates in sodium montmorillonite, forming ordered water lattices that both produce swelling pressure when less than three hydrates have been formed, and offer resistance to shear. Interlamellar sodium ions may only serve to balance crystal lattice charge deficit. In contrast, bivalent interlamellar cations merely serve to balance charge deficits and are associated with water molecules that are not organized but form a two- dimensional aqueous solution. If this is the case, the shear strength expressed in terms of internal friction should be appreciably less for calcium than for sodium montmorillonite clay. This is true as documented by triaxial shear tests, which gave the figure 9^{o} for sodium and 5^{o} for calcium smectite clays at normal pressures exceeding 200 kPa (18,19).

2.3.4.3 Information deduced from rheological tests

Since about 1960 a number of reports based on the application of Rate Process Theory for evaluation of the nature of interparticle bonds in soils have been published. The investigators have all used Eyring's idealized model for neighboring plane layers of molecules sliding past each other for the formulation of creep equations, usually implying that constant creep rate is proportional to the product of the number of interparticle bonds, the displacement of each bond in the direction of the shear stress, and the frequency of rupture of a single bond. The resulting expression for the net frequency of molecular jumps in the direction of shear thus has the form (20):

$$\vec{\nu} - \overleftarrow{\nu} = 2\ kT/h\ \exp(-\Delta F/RT)\ \sinh\ (f\lambda/2kT) \quad (4)$$

where ν = activation frequency
k = Boltzmann's constant
T = Absolute temperature
h = Planck's constant
R = Universal gas constant
ΔF = Activation energy, i.e. energy required to displace a mole of flow units from the current to the neighboring equilibrium position

λ = distance between two neighboring equilibrium positions

f = molecular-level driving shear force on flow unit

The problem in using Eq.4 for evaluating the bond strength is that creep results not only from the integrated displacement of flow units, the definition of which is not simple, but also from microstructural changes, i.e. altered particle arrangement and character of particle contact, which take place at a decreasing rate when the shear stress is below a critical level. Microstructural changes were considered by Kuhn (21) who assumed the activation energy to be constant, and making use of Cundall and Strack's stress partition model of contacting discs, he found the theoretically derived creep rate to be consistent with actually recorded creep for an activation energy of 25 kCal/mole. He assumed the particle diameter to be 1 μm and λ to be 2.8 Å, which is hardly applicable to smectite clays because the stacks, i.e. the particles, are anisometric with a thickness of 5×10^{-3} to 2×10^{-2} μm.

A fundamental shortcoming of all the models is the assumption that there is only one type of bond, i.e. one single activation energy. It is in fact clear that quite different types of bonds are operative simultaneously in any clay and for smectites this can be examplified by the conditions in Na montmorillonite stacks with 1 hydrate and with 2 or 3 hydrates, respectively, giving the stacks different stress/strain properties, and in the contact regions of neighboring stacks, where van der Waals, hydrogen, electrostatic, and primary valence bonds operate simultaneously. A further defect is the assumption of flow units of uniform type since they do in fact vary in size, shape and character, from individual atoms at the points of mineral contacts to large patches of water molecules.

While the aforementioned attempts of evaluating the type of particle bonds from Rate Process Theory suffer from several oversimplifications and incorrect assumptions, there are possible ways of getting at least an idea of the interparticle bonds. This can be made by applying a creep model developed by Feltham and based on stochastic mechanics (22). It has been taken as a basis of a general creep model which appears to be compatible with both microstructural processes and recorded creep strain (23).

Following Feltham creep can be modeled as the integrated migration of a population of dislocations or of a particle assemblage under the influence of a shear stress. The displacement of the individual units is controlled by the energy barrier level that it has to overcome, and the net strain is thus determined by the actual barrier spectrum and of the distribution over the barrier spectrum of units that have already overcome a barrier. The following assumptions can be made:

1. The probability of a flow unit to overcome a barrier at which it is temporarily stopped, is given by the expression:

   $$P \text{ (single transition)} = \exp(-u/kT)$$

   where u = Barrier height
   k = Boltzmann's constant
   T = Absolute temperature

2. A flow unit makes ν attempts per second to overcome "its" barrier, i.e. ν is the vibratory frequency

3. The flow units are initially uniformly distributed over the assumed barrier spectrum

4. Flow units that overcome "their" barriers become distributed in one of the following four manners:

   * The unit is held up at the next lower energy barrier. Units that overcome the lowest level leave the system ("Cascade")

   * The unit is held up with the same probability at the next lower and next higher level. Units that overcome the lowest level leave the system by 50 % probability. Those which overcome the highest level are held up at the next lower level with 100 % probability ("Diffusion with sink")

* As the previous one but no units are assumed to leave the system ("Diffusion without sink")

* The units are held up with equal probability at any level ("Landau")

Computer calculation using a program developed within the project has been applied to illustrate the successive redistribution of energy levels for all the cases and no significant difference has been found, meaning that the redistribution criteria are not critical to the validity of the creep model. Fig.16 illustrates the successive redistribution to various energy levels for the cases "Diffusion with sink" and "Landau" considering the energy interval 0.8 - 1.8 eV, which roughly covers the range from strong hydrogen bonds to primary valence bonds. The initial number of flow units, termed dislocations in the graphs, was arbitrarily taken as 10 000, and the number of energy barriers as 20 and neither of these figures are critical to the outcome of the study. The vibratory frequency $\nu=10^{12}$ is of actual magnitude.

The vertical axis of the diagrams in Fig.16 represents the total number of barrier climb per second and if one assumes that the variation in strain associated with each jump does not vary too much, the jump rate should thus be approximately proportional to the bulk strain rate. Fig.17 shows computer-simulated creep curves for three of the distribution models, which all exhibit the characteristic shape of recorded creep of non-cemented smectite clays (cf Fig.18), i.e. with the curved initial part that is represented by t_o in the gene-

ral expression of angular strain (24):

$$\gamma = B \ln(t+t_o) + A \qquad (4)$$

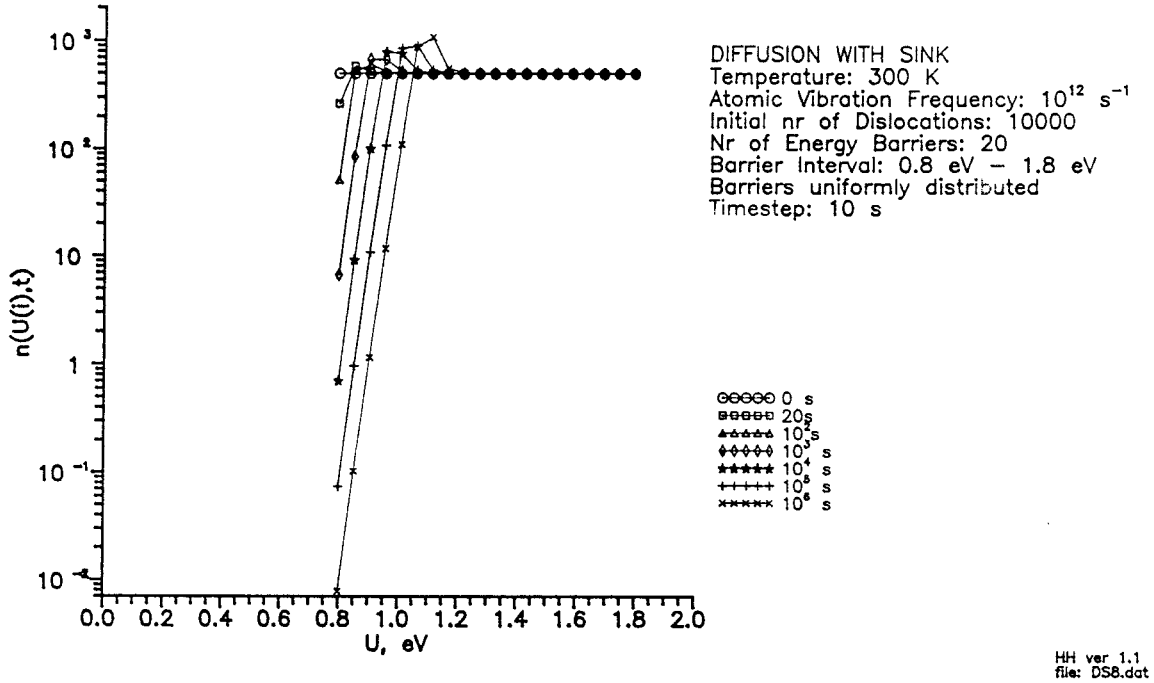

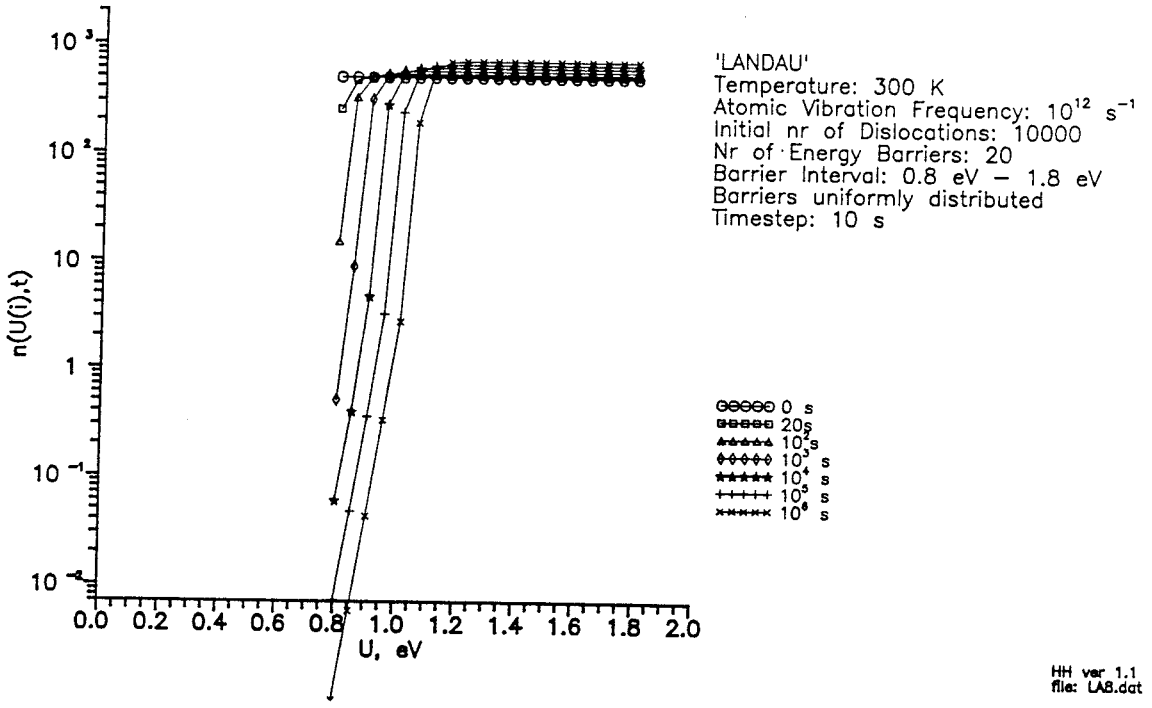

Fig.16 Flow unit distribution over barrier spec- 0.8-1.8 eV after onset of creep

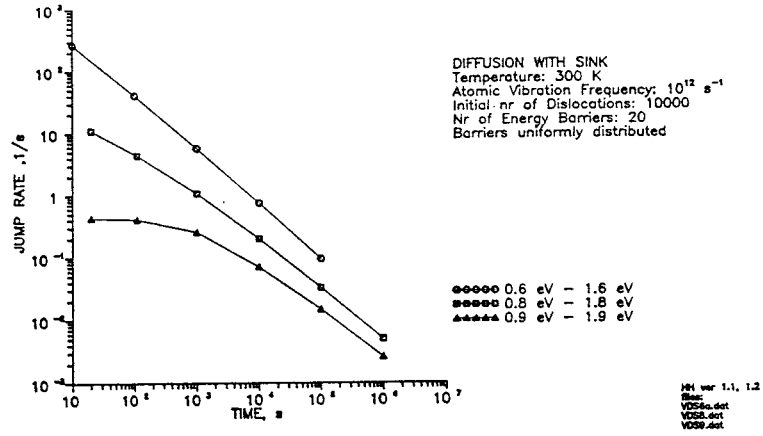

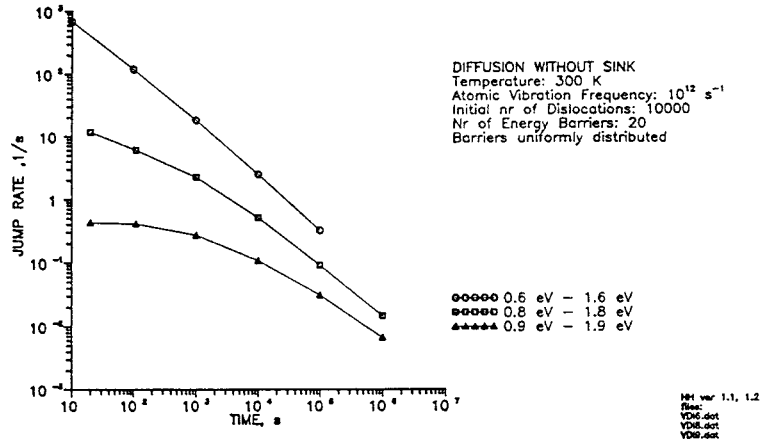

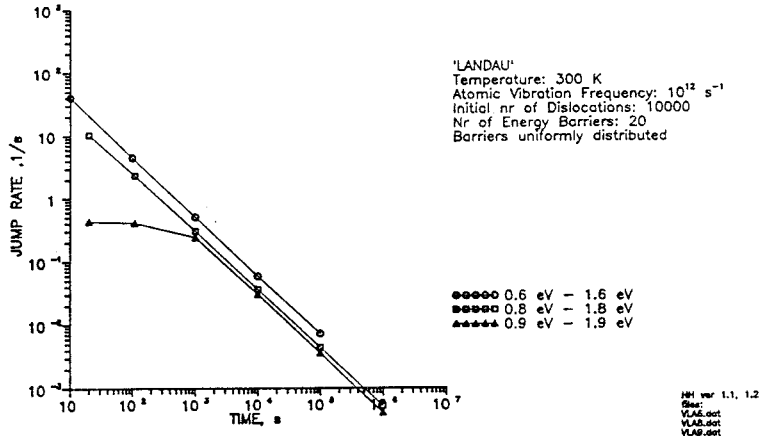

Fig.17 Number of barrier climbs after onset of creep for different distribution models

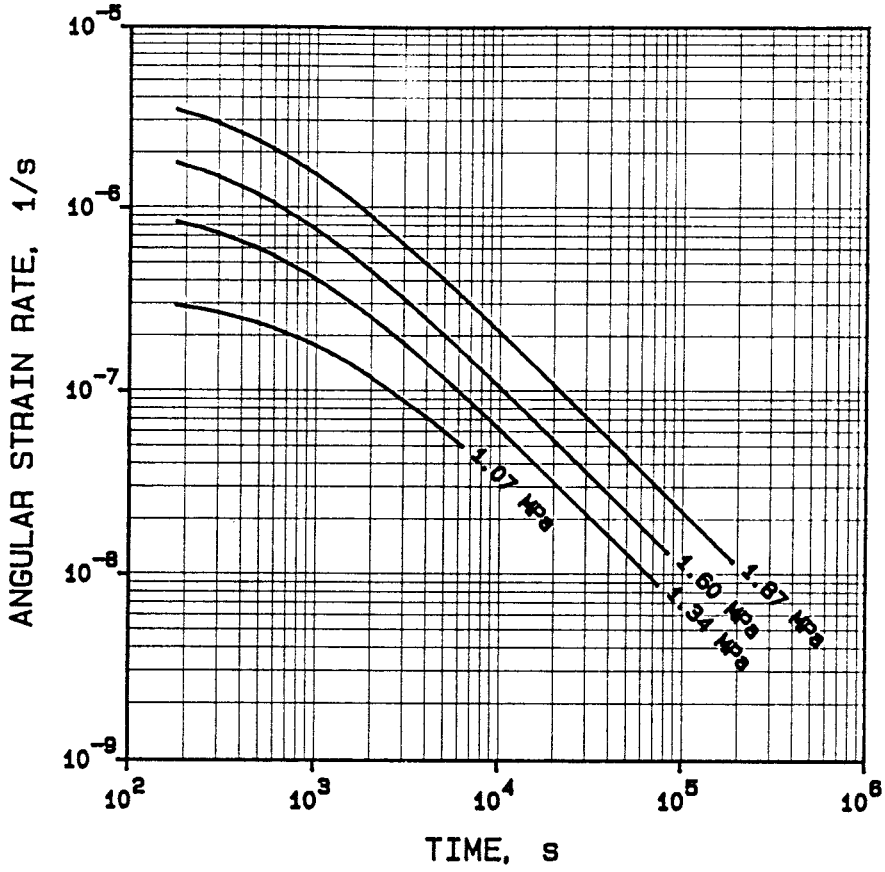

Fig.18 Strain rate versus time of MX-80 clay

One finds that the initial strain is very rapid and that it approaches log time creep behavior very quickly when the spectrum contains weak bonds (low barriers), while this approach is very much slower and yields the curved shape when the energy interval is higher.

The study supports the belief that creep in soils can be regarded as a thermally assisted slip of flow units over energy barriers represented by a spectrum of interparticle and intraparticle bonds. One concludes that a whole range of bonds exist in clays, where the weakest ones are represented by van der Waals forces and weak hydrogen bonds operating in the contact regions of neighboring stacks,

and the strongest ones being primary valence bonds between mechanically interacting flakes. The rest of the spectrum is probably dominated by medium and strong hydrogen bonds.

It should be added that a way of illustrating the creep process is offered by a simple version of Eyring's rheological model with a non-linear viscous element that is characterized by a linear increase in viscosity with time (Fig.19). Like all other rheological models it does not reveal the strain-generating mechanisms but serves to quantify major parameters, in our case t_o and B (24). The appearance of creep curves generated by the rheological model is obvious from the diagram in Fig. 19.

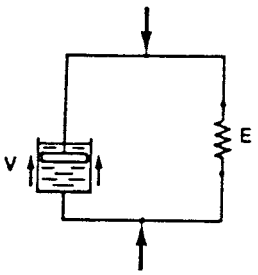

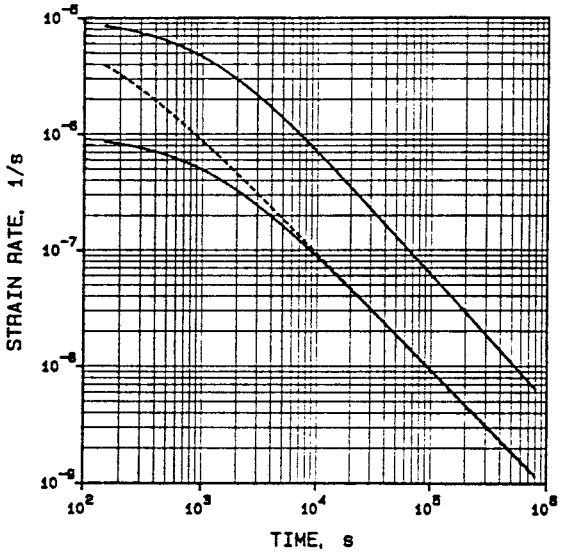

Examples of the appearance of creep curves according to the simplified Eyring/Kelvin model,Fig 55. The three curves are characterized by the following sets of data:

Upper: $E = 10^7$ Pa, $\eta_o = 10^{11}$ Pas, $a = 10^8$ Pa, $t_o = 10^3$ s
Central: $E = 10^7$ Pa, $\eta_o = 10^{11}$ Pas, $a = 10^9$ Pa, $t_o = 10^2$ s
Lower: $E = 10^7$ Pa, $\eta_o = 10^{12}$ Pas, $a = 10^9$ Pa, $t_o = 10^3$ s
σ_o is taken as 1 MPa in all the cases

Fig.19 Simple version of Eyring's model and typical curves for characteristic smectite clay material properties

3 GENERAL MICROSTRUCTURAL MODEL (GMM)

3.1 Introduction

The understanding of transport phenomena, alteration processes, and rheological behavior of smectite clay formed through water uptake by confined granular, commercial bentonite powder, requires access to a microstructural model describing both geometrical features and force fields on a microscopic scale. A first version of such a model was outlined some years ago, based on preceding studies of illitic clays, and it is currently being refined, taking into account recent results from both microscope studies and various physical tests. Its present form will be given in this report, in which the smectite mineral family will be represented by montmorillonite.

We will consider first a basic version of the GMM which is related to room temperature and low or moderate salt porewater, and continue by introducing effects of very salt water. Finally, we will consider the influence of higher temperatures.

3.2 Basic GMM version

3.2.1 *Evolution of clay microstructure*

The basic idea is that the clay microstructure, which is initially formed by the powder granules, successively transforms to a more homogeneous state by redistribution of both clay flakes and water (Fig.11), cf.(25). A major process is concluded to be the foliation of thin stacks from the dense granules and creation of more or less soft gels in the voids between the granules (Fig.20). These voids, termed external, are of various size and they are

stochastically oriented in space and combine to form 3-dimensional crankshaft-like patterns of the type shown in Fig.21 rather than straight capillaries. This yields a total flow length of about 3 times the net flow length in the direction of the hydraulic gradient as found by applying stochastic theory (26), and this has been accounted for in GMM. The model also has the characteristic feature that the system of external voids, being completely interconnected prior to hydration, retains a substantial degree of interconnectivity also after swelling of the initially dense granules. It is thus assumed that practically no voids become completely sealed off from neighboring ones and that no individual passages have dead ends.

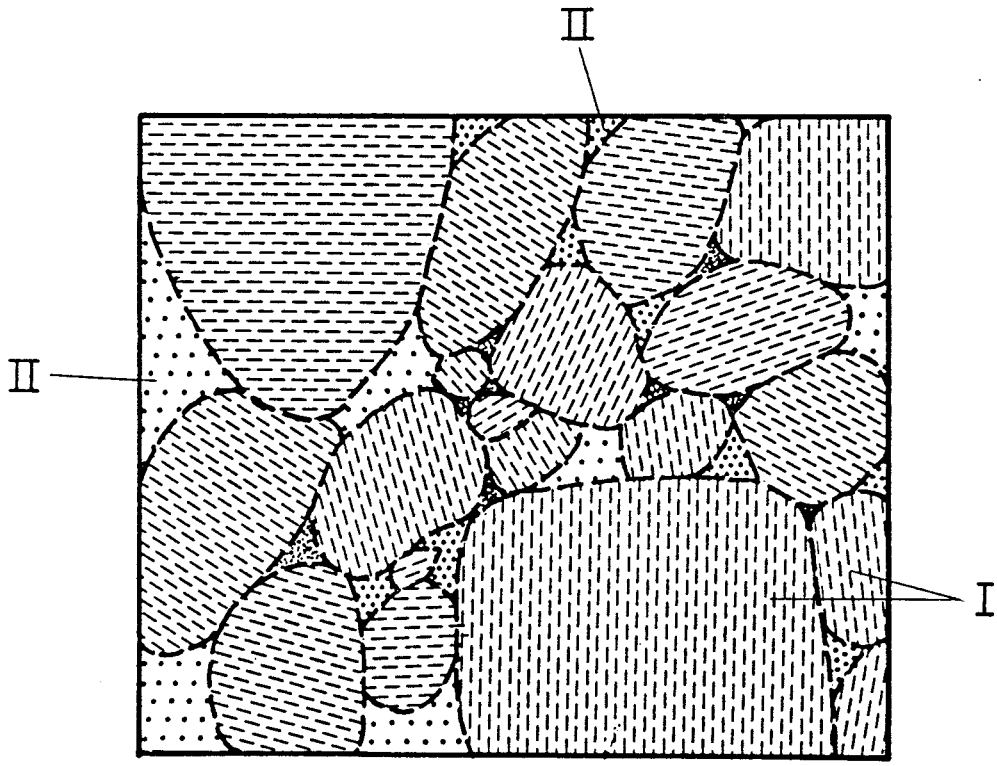

Fig.20 Generalized microstructural pattern of Na montmorillonite clay formed from powder grains. "I" is expanded grain (1-3 interlamellar hydrates), "II" external pores with gels of different densities

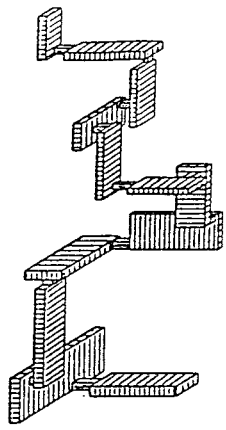

Fig.21 Passage of external voids in 3D view

It can be assumed that a certain fraction of the stacks are prevented from moving freely or from expanding by precipitations that are either inherited from the natural bentonite strata or formed by the heating and other activities involved in the industrial processing. Thus, it is anticipated that mechanical strain, induced by shearing the water saturated system of granules that forms the "artificial" clay that we are dealing with here, or caused by thermomechanical effects on heating the clay, will activate such stacks and alter the microstructure. We will see later that this effect is of importance for the physical properties of thermally matured clays.

High voltage electron microscopy of nearly water saturated Na montmorillonite clay gels has verified that the large majority of the flakes that constitute the stacks do not separate spontaneously after the maximum expansion that the stacks can undergo, and which corresponds to three interlamellar hydrate layers (27). The stacks contain a number of flakes which is in the range of 3 to 50, a probable average for montmorillonite in Na form being 5, while the number probably averages at 20 when the clay is in calcium form.

The basic principle of the derived model of Na montmorillonite is that the virgin system of confined powder granules forms a matrix in which the stacks expand to hold 1 to 3 interlamellar hydrated layers, depending on the density, and give off stacks of flakes with 3 interlamellar hydrates that create gel fillings in the voids between the grains. These gels are assumed to have a more or less cardhouse-like structure as suggested by electron micrographs and this may be explained by the dominant type of particle bonding in gels formed by coagulation of polarized particles that are free to move, i.e. in our case presumably electrostatic attraction of the positively charged edges to the negatively charged basal planes of neighboring stacks. Actually, similar arrangements may also result from foliation of thin stacks from the primary, dense groups of stacks that constitute the granules without passing through a stage of liberation. Stack arrangements of this type are represented by drawings e), f), and g) in van Olphen's classical set of particle association modes shown in Fig.22.

Naturally, the gels formed in the voids are not characterized by good ordering of the stacks but the essential microstructural features of the matured clays can probably still be described by applying the card house geometry, which makes it possible to treat transport problems quantitatively.

3.2.2 *Exchange of external and internal water*

A matter of profound importance for the derivation of a general microstructural model is the coupled hydration and regrouping of particles that ultimately yield an equilibrium state. The processes are transient and the time to obtain equilibrium

very long as concluded from many kinds of laboratory tests. The fact that water migration and successive establishment of ordered water structures is involved is very clearly demonstrated by proton NMR tests performed by Carlsson (17).

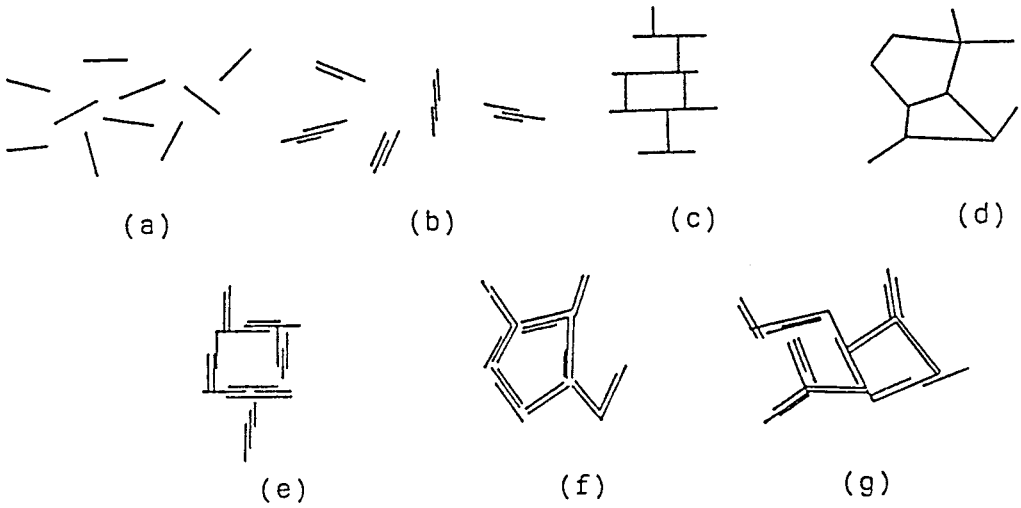

Fig. 22 Various modes of particle association (after van Olphen).

a) Dispersed and deflocculated. b) Aggregated but deflocculated. c) and d) flocculated with edge/face and edge/edge association, respectively. e), f), and g) flocculated and aggregated with different edge/face and edge/edge associations

Carlsson recorded the relaxation time T_2 of freshly prepared MX-80 clay powder mixed with distilled water over two to four months long periods and found that T_2 increased successively for very soft

clay gels, indicating considerable microstructural changes in the form of slow establishment of an open gel structure with very much external and very little internal, ordered water (Curve A in Fig.23).

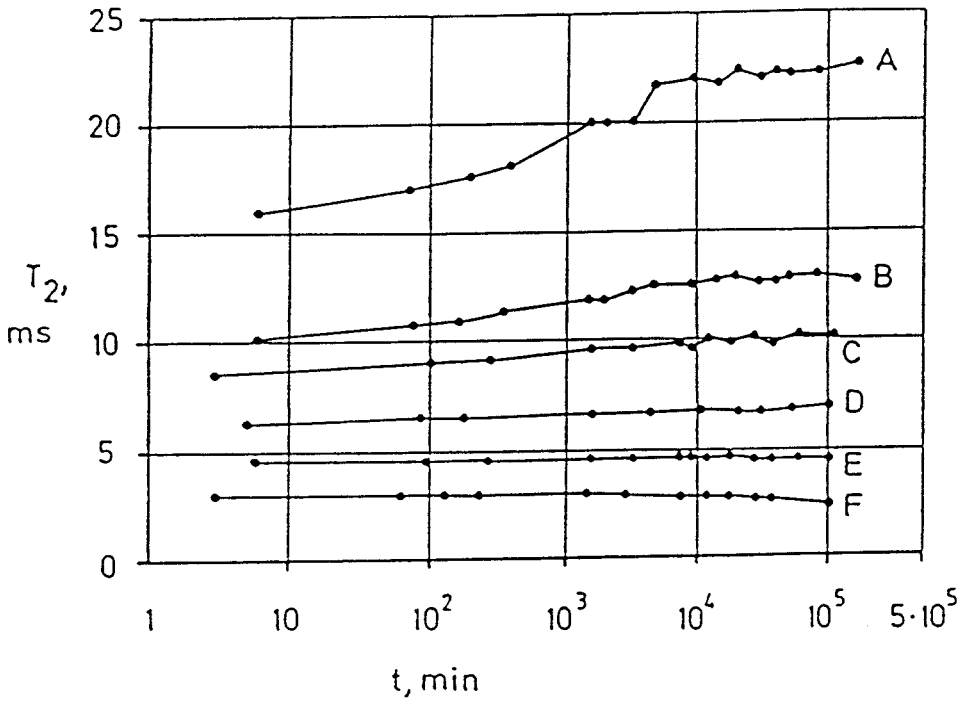

Fig.23 Relaxation time of MX-80 clay mixed with distilled water. A: water content w=1500 %, B: w=790 %, C: w=600 %, D: w=430 %, E: w=300 %, F: w=190 %

For somewhat denser but still very soft clay, Carlsson found that T_2 tended to drop with time, indicating that the increase in ordering of the interlamellar water dominated over the successive growth of external water caused by the "aggregation" process (Curve F).

3.2.3 *Hydraulic conductivity of GMM clay*

3.2.3.1 Gel densities

For quantification we will refer to three standard clays termed A, B, and C with the properties given

in Table 5, assuming them to be formed from finely granular MX-80 bentonite powder (25). The grain size distribution of the granules is not critical to the validity of the model because large grains break down to finer ones on compaction or wetting. It is therefore reasonable to apply log normal distributions of the void size and maximum void size data derived from studies of the MX-80 powder.

Table 5. Reference clays A,B,C

Clay	Density (sat.) g/cm^3	Dry density g/cm^3	Water cont. %
A	2.13	1.79	19
B	1.85	1.35	37
C	1.57	0.90	73

As to the gels formed in the voids, high voltage electron microscopy of hydrated Na montmorillonite gels (27) and comprehensive TEM studies of impregnated soft natural smectite sediments (28) indicate that very soft unconsolidated gels form cardhouse-like structures with an average spacing of the thin expanded stacks of a few hundred to a few thousand Å. Estimates of the density of the clay gels related to the bulk density of the total mass have led to the figures given in Table 6, which specifies average gel densities as functions of the size of the external voids between fully expanded granules.

Table 6. Distribution of clay gel densities, g/cm^3

Clay	Bulk density g/cm^3	Diameter of external voids, μm		
		1 - 5	5 - 20	20 - 50
A	2.13	1.3	-	-
B	1.85	1.3	1.2	-
C	1.57	1.3	1.2	1.1

3.2.3.2 Microstructural properties of the void-filling clay gels

For evaluating the hydraulic conductivity of the clay gels formed in the external voids, we will use van Olphen's type e) as a prototype unit of the gel microstructure and assume here that it is cubical with a free inner side length d_1 and that its particle components consist of fully hydrated smectite stacks with a thickness termed x (cf. Fig.23). Referring to the three gel densities given in Table 6, we arrive at the corresponding d_1- values in Table 7 for the ideal Na smectite material that we are presently considering. The calculations are based on the assumption that each stack consists of 3 fully hydrated flakes, i.e. with 3 interlamellar hydrate layers. The thickness of each hydrated stack is then about 50 Å.

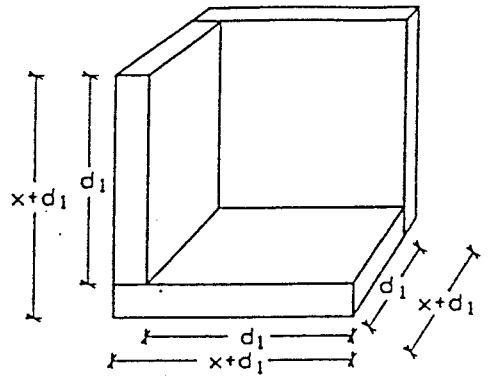

Fig.23 "Unit" cell of clay gel

Table 7. Free space d_1 of cubical "unit" cell of Na montmorillonite gel

Gel density g/cm^3	d_1 Å
1.3	341
1.2	567
1.1	1232

Some further quantifications regarding the gel microstructure are required: We will assume here that the entire gel microstructure consists of continuous passages with no dead ends but with a regular change in width from the "full-sized" opening d_1 of the cubical inner space, to an assumed "critical" opening size d_2 (Fig.24). For quantification we need to know both d_1 and d_2 and the fraction length n_1 that is taken up by the full size openings per unit passage length. For Na montmorillonite it is estimated that d_2 can be taken as one quarter of d_1, and n_1 as 90 % . For further mathematical treatment we introduce also $n_2 = 1 - n_1$.

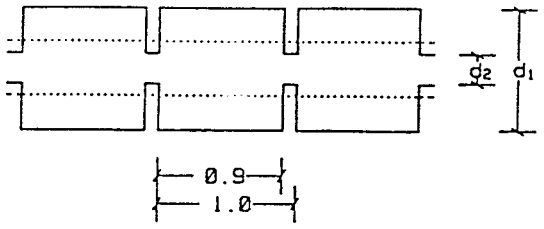

Fig.24 Schematic passage of regularly varying width in Na clay gel filling. The depicted geometry implies $d_2 = 0.25\ d_1$, and $n_1 = 0.9$

3.2.3.3 Equivalent diameter concept

For a circular tube of varying diameter, the Hagen-Poiseuille law states for the pressure drop ΔP:

$$\Delta P = \Sigma \Delta P_i = q \cdot \frac{128\ \gamma}{\pi} \cdot \Sigma \frac{l_i}{d_i^4} \qquad (5)$$

Where

ΔP_i = Pressure drop across tube section with length l_i and diameter = d_i
q = flow through tube
γ = dynamic viscosity of fluid

A capillary tube of length $L = \Sigma l_i$ and with constant aperture should, in order to give the same flow for the same pressure drop, be assigned an equivalent diameter d:

$$\frac{L}{d^4} = \Sigma \frac{l_i}{d_i^4} \qquad (6)$$

For the schematic case in Fig.24 with two discrete diameters d_1 and d_2, Eq.6 could be rearranged to calculate the equivalent diameter d:

$$d^4 = \frac{d_1 \cdot d_2}{n_1 d_2^4 + n_2 d_1^4} \qquad (7)$$

where n_1 and n_2 denote fractions of the tube length taken up by openings sized d_1 and d_2, respectively. In most cases an approximate expression can be used to calculate the equivalent diameter d:

$$d = d_2 \cdot (n_2)^{-\frac{1}{4}} \qquad (8)$$

Hence, the equivalent diameter d is proportional to

whereas the fraction n_2 is less significant.The equivalent diameters of gels with the three densities previously considered are shown in Table 8 and using these figures and Eq.5 one arrives at the theoretical gel conductivities shown in Table 9.

Table 8. Diameter d of capillary passages through Na clay gel fillings

Gel density g/cm^3	d Å
1.3	150
1.2	250
1.1	500

3.2.3.4 Conductivity of soft gel fillings

The calculation of the hydraulic conductivity of the soft clay gels can be made by use of the capillary diameters in Table 8, which can be taken as a basis for estimating the integration interval that is required as input for the calculation of conductivities using the expression in Eq.9. The distributions chosen here are shown in Fig.25.

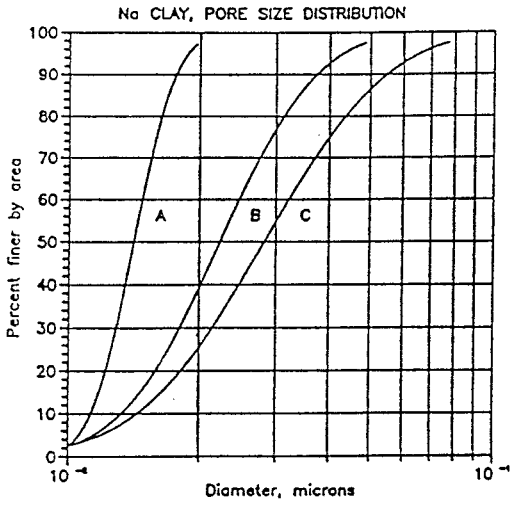

Fig.25 Distribution of pore cross section area for gels with the densities 1.1, 1.2, and 1.3 g/cm^3

$$k = \frac{p \cdot \Pi \cdot g \cdot \rho}{128 \cdot h} \int_{x_1}^{x_2} n(x) \cdot x^4 \cdot dx \qquad (9)$$

where x_2 = upper diameter limit
x_1 = lower diameter limit
$n(x) \cdot dx$ = number of pores per unit pore cross section area in the diameter range (x, $x + dx$)
p = porosity
g = acceleration of gravity
ρ = density of fluid
η = dynamic viscosity of fluid

n(x) is determined by assuming log normal distribution of the pore cross section area. For the purpose of evaluating Eq.9, a computer code with input parameters as listed below, has been developed:

* lower and upper limit of integration (microns)
* mean diameter (microns)
* standard deviation (powers of ten)
* porosity

Means and standard deviations were determined by postulating that the range of integration should correspond to 4 units of standard deviation. Using the distribution functions of Fig.25 and the porosities of Table 9, which were derived from the gel densities but corrected for the conversion to constant aperture tubes, we arrive at the hydraulic conductivity values of Table 10. The hydraulic conductivities were calculated using the multiplication factor 0.5 to account for deviation from the assumed circular cross section.

Table 9. Effective porosities of soft clay gels

Density, g/cm^3	Porosity
1.3	0.14
1.2	0.17
1.1	0.20

Table 10. Hydraulic conductivity of clay gels formed by foliating stacks which fill up the external voids

Density, g/cm^3	Calculated hydraul. conductivity, m/s
1.3	0.4×10^{-11}
1.2	2.1×10^{-11}
1.1	9.8×10^{-11}

Clays prepared with a bulk density of 1.1 - 1.3 g/cm^3 have actually been tested and found to yield conductivities that are somewhat higher than the theoretically derived ones but since such clays are characterized by scale-dependent structural heterogeneities, which unevitably raise the bulk conductivity, the values in Table 10 are still reasonable.

3.2.3.5 Conductivity of reference clays

The conversion of actual pore passage geometry to tubular shape allows for determination of the average hydraulic conductivity of our reference clays by using the capillary flow model, provided that the range of equivalent diameters can be estimated. This can be made on the basis of the data given earlier, from which it is estimated that the dia-

meter ranges between 0.01 and 0.02 microns for Clay A, while for Clay B the interval should be 0.01 - 0.05 microns. For the soft Clay C the corresponding range is 0.01 - 0.08 microns. For a system of straight, continuous, capillary tubes the Hagen-Poiseuille law can be employed to derive an expression to compute the hydraulic conductivity as in the case of the soft clay gels.

In the case of for instance clay A with diameters ranging between 0.01 and 0.02 microns, the standard deviation would thus be $0.25 \cdot \log(0.02/0.01) = 0.07526$ powers of ten and the mean $0.01 \cdot \sqrt{0.02/0.01} = 0.0141$ microns.

The diameter distributions used for our calculations are shown in Fig.26.

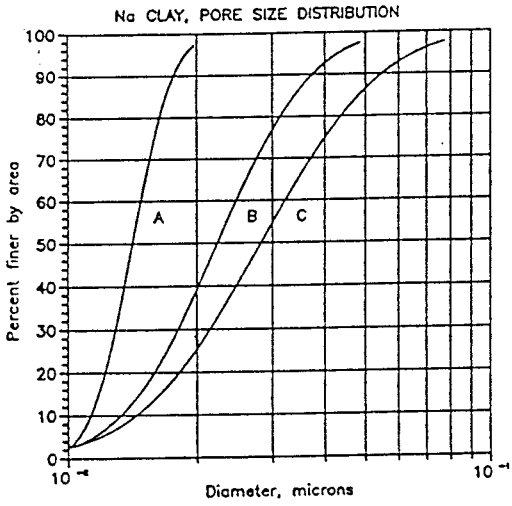

Fig.26 Distribution of pore cross section area for clays A, B and C (Na state)

The input parameter 'porosity 'is determined by the effective porosity of the reference clays corrected

with respect to the porosity of the clay gel fillings in the external pores, which in turn has to be corrected for the conversion of the gel voids to constant aperture tubes. The calculation of these corrections are purely geometrical and need not be discussed here. The resulting porosities are listed in Table 11.

Table 11. Corrected porosities to be used in conductivity calculations

Clay	Correction	Input porosity
A	0.14	0.015x0.14 = 0.0021
B	0.17	0.050x0.17 = 0.0085
C	0.20	0.370x0.20 = 0.0740

While the soft gel fillings are supposed to have a fairly open structure, which allows for approximately straight flowpaths, this is not the case for the system of external pores in which the clay gels are confined. The afore-mentioned correction for the tortuous passages, i.e. the crankshaft-type geometry, has therefore been applied, meaning that the flowpaths on the average will be aligned along the direction of the hydraulic gradient for 1/3 of its length, i.e. the value calculated according to Eq.9 has been divided by 3. Table 12 shows the calculated conductivities of the reference clays.

Table 12. Theoretical, average hydraulic conductivity of reference clays A,B ,and C (Na state)

Clay	Bulk density g/cm^3	Eff. porosity	Average hydr. conductivity, m/s
A	2.13	0.015	2.1×10^{-14}
B	1.85	0.050	2.6×10^{-13}
C	1.57	0.37	4.3×10^{-12}

The theoretically derived conductivities are plotted in Fig.27, which also shows the generalized relationship between bulk density and empirically recorded values and we conclude from the close agreement that the flow model operates satisfactorily for Na smectite.

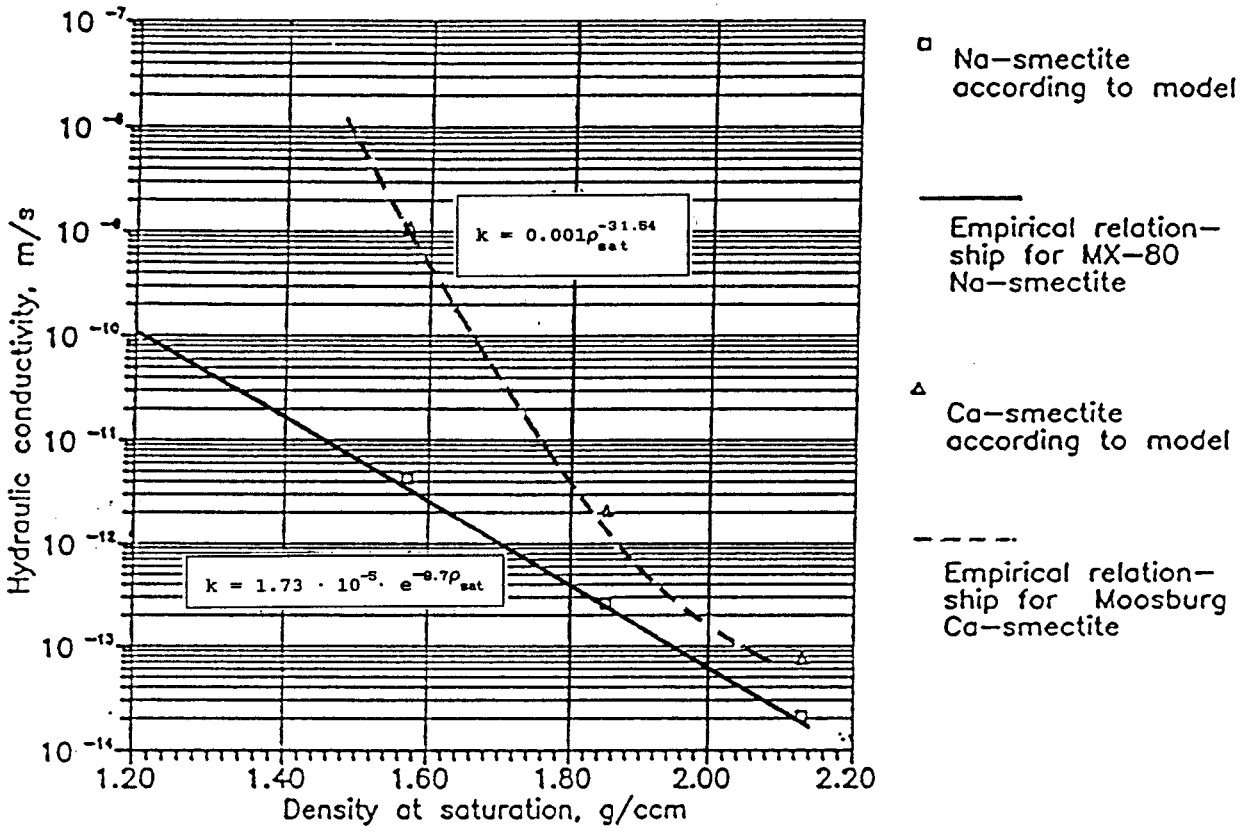

Fig.27 Theoretical and empirical relationships between bulk hydraulic conductivity and bulk density (Na and Ca states)

Considering now the same reference clays formed from Ca saturated clay powder there are two fundamentally different properties, namely that only two hydrates can be established in the interlamellar space and that the number of flakes in the stacks is considerably higher in Ca montmorillonite. This means that the granules forming the initial particle system expand less than in the sodium case and that the exfoliation of stacks from the

granules and the formation of gels in the external pores are also less effective, especially in the widest voids. For clays A and B the densities of the softest gels in external voids are assumed to be about the same as in the sodium case, i.e. they are taken to be 1.3 and 1.2 g/cm^3, respectively. For clay C the gel density is assumed to be as low as 1.05 g/cm^3 in the widest voids because the poor expandability is concluded to yield a considerable heterogeneity of the gel and therefore a low average density.

As to the number of flakes per stack it is assumed that while this number may well be 10 or higher than that in the granules with their inherited internal structure, mechanical strain in the exfoliation process results in thinner stacks forming gels. Hence, gels with a density of 1.2 and 1.3 g/cm^3 are assumed to be characterized by cardhouse-arranged stacks of 5 flakes and a thickness of 80 Å. Gels with a density of 1.05 g/cm^3 are stable only when confined in voids and not in bulk, and since exfoliation takes place with only minor hindrance in the largest voids they are assumed to consist of stacks that hold 10 flakes or even more than that. Taking the average number to be 10, the stacks have a thickness of about 160 Å and using these data we arrive at the d_1 spacings shown in Table 13.

Table 13. Free space d_1 of cubical "unit" cell of Ca smectite gels

Gel density g/cm^3	d_1 Å
1.3	700
1.2	1100
1.05	10000

For further derivation of the model the same d_1/d_2 ratio can be applied in the calculation of the diameter of the equivalent capillaries as for the Na smectite gels, provided that the Ca gel density is 1.2 g/cm^3 or higher. For the softest gel, i.e. the one with 1.05 g/cm^3 density, d_1 approaches the maximum flake length and this implies a more open structure and it is assumed here that $d_2 = 0.5\ d_1$ is a characteristic feature. With the given conditions, the diameters of the equivalent capillaries shown in Table 14 are obtained.

Table 14. Diameter d of capillaries of Ca clay gels

Gel density g/cm^3	d Å
1.3	310
1.2	500
1.05	8000

The hydraulic conductivity of the three reference clays can now be calculated using the computer code described in the previous section. The diameter values for input as upper and lower limits of integration can be estimated from Table 14: For clays A, B and C the ranges used are: 0.01-0.05 microns, 0.01- 0.08 microns and 0.01-1.2 microns, respectively. Means and standard deviations can be taken as for the Na-saturated clays, i.e. the range of integration should correspond to four units of standard deviation, with the mean symmetrically centred in the logarithmic interval. The distributions used in the calculations are shown in Fig.28.

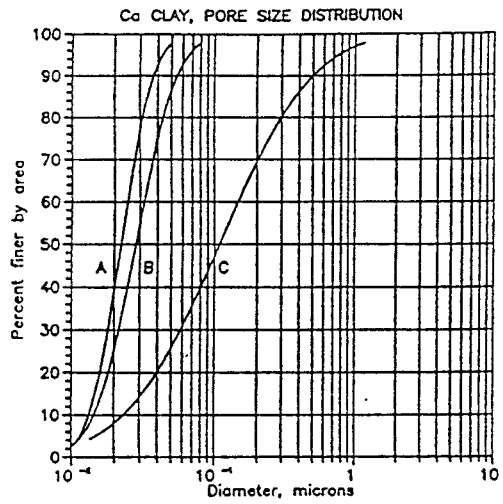

Fig.28 Distribution of pore cross section area for clays A, B and C (Ca state)

Since the calcium smectite grains do not expand beyond two interlamellar hydrate layers we will use the earlier derived effective porosity data for this expansion stage. As for the Na-saturated smectite, corrections for gel porosity and for the conversion to constant aperture passages need to be made, yielding the porosities for use as input parameters in the calculations being shown in Table 15.

Table 15. Corrected porosities to use for conductivity calculations

Clay	Correction	Input porosity
A	0.16	0.015x0.16 = 0.0024
B	0.18	0.200x0.18 =0.0360
C	0.62	0.470x0.62 =0.2900

Making the same corrections for deviation from circular cross sections and straight flowpaths as in the case of Na saturated smectite, we arrive at the hydraulic conductivities shown in Table 16.

Table 16. Theoretical, average hydraulic conductivity of the reference clays A, B, and C (Ca state)

Clay	Bulk density g/cm^3	Eff. porosity	Average hydraul. cond., m/s
A	2.13	0.015	7.5×10^{-14}
B	1.85	0.200	2.1×10^{-12}
C	1.57	0.470	1.1×10^{-9}

The theoretically derived conductivities are plotted in Fig.27, which also shows the generalized relationship between bulk density and the hydraulic conductivity that are found to be representative of a typical Ca smectite-rich material (Moosburg). It is clear from the satisfactory agreement between the theoretically deduced conductivities and the recorded ones *both for Na and Ca states* that the flow model works and that the basic GMM accounts for microstructural control of water flow.

The relationship between hydraulic conductivity on percolation with water of low ionic strength, and bulk density, can be expressed in the following way for clays saturated by sodium and calcium (cf. Fig.27):

Na montmorillonite clay: $k = 1.73 \cdot 10^{-5} \cdot e^{-8.7\rho_{sat}}$ m/s (10)
$(1.2 < \rho_{sat} < 2.1\ g/cm^3)$

Ca montmorillonite clay: $k = 0.001\rho_{sat}^{-31.54}$ m/s (11)
$(1.5 < \rho_{sat} < 2.1\ g/cm^3)$

3.2.3.6 Uniformity of water percolation

The stochastic character of the microstructural constitution implied by GMM suggests that the distribution of flow through clays of this sort is very heterogeneous. Thus, Fig.29, which gives the approximate relative amounts of microstructural units of the reference clays, demonstrates that the permeable fraction of a cross section of denser clay is indeed very small. The actual, theoretical variation in flow rate is illustrated in Fig.30 from which it has been concluded that the high rates in the widest external voids in clays with a dry density of less than 1 g/cm^3 may cause erosion and piping due to breakdown of the soft gels in these voids at higher hydraulic gradients than around 50 (25).

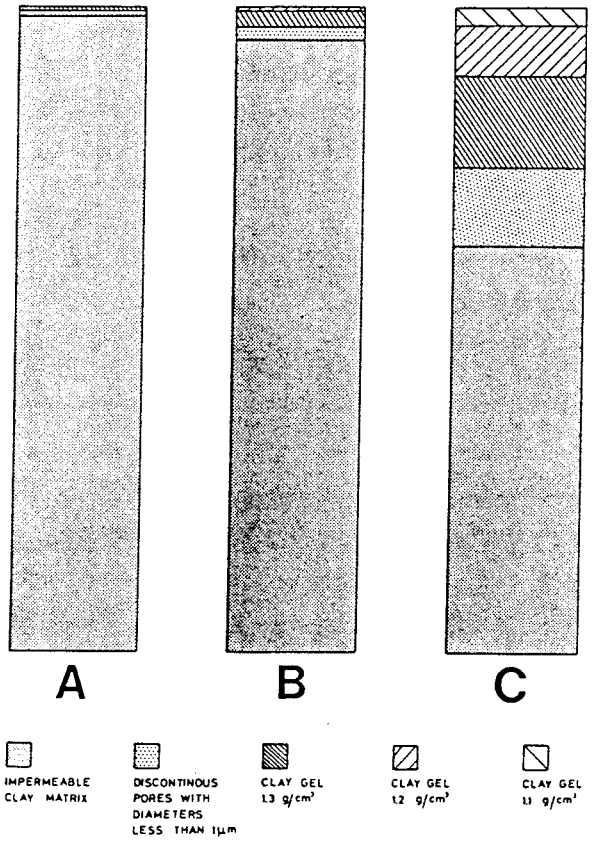

Fig.29 Relative amounts of microstructural units in the reference clays (A; ρ_d=1.8 g/cm^3, B; ρ_d=1.35 g/cm^3, C; ρ_d=0.9 g/cm^3), (25)

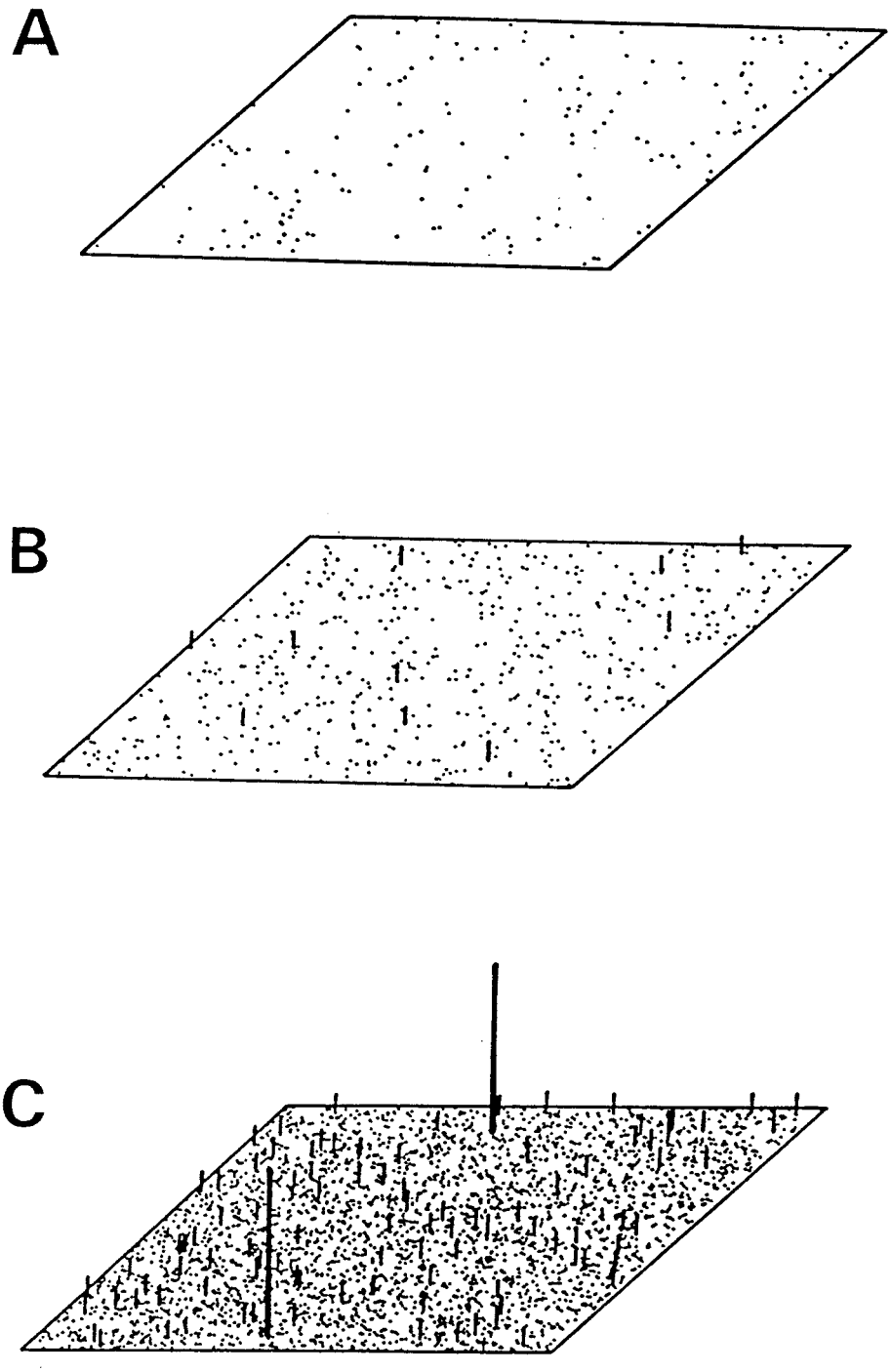

Fig.30 Flow rate distributions in clays A,B, and C. Dots are 1-5 μm gel-filled voids, short bars 5-20 μm voids and long bars 20-50 μm voids (25). (250x250 μm element)

3.2.3.7 Influence on hydraulic conductivity by porewater electrolytes

It has been mentioned earlier in the text that the interlamellar spacing is not or very little affected by the cationic strength as demonstrated by XRD tests on montmorillonite soaked with water that has a salinity of approximately that of the oceans. At much higher electrolyte concentrations, for example if montmorillonite clay is contacted with brines, the interlamellar spacing may be reduced due to dehydration. We will consider here only salinities that are relevant to Swedish conditions and have taken NaCl and $CaCl_2$ solutions with a concentration of 100 % as an upper limit.

While the stacks are not significantly affected by high salinities, the gels formed in the external voids are influenced in two ways, i.e. by forming stronger aggregate networks that consist of thicker stacks than in electrolyte-poor water. The reason for the higher strength is that the interparticle forces are stronger, primarily through more effective Coloumb attraction and less effective double-layer repulsion, while the thicker stacks are assumed to result from less powerful dispersion of stacks from the granules.

These estimates are supported by Tessier's finding that, for Na montmorillonite, the number of flakes in distilled water is around 5 in most stacks, while this figure increases to 10-15 in brackish water and 20 or more in NaCl solution with a concentration of 2.8 % (29). The release of stacks from the granules in maturing bentonite clays is associated with mechanical strain and the average number of flakes in the stacks is therefore probably not more than 10 and using this figure as an upper limit, and assuming that the extension of the electrical double-layers between adjacent stacks to

be a measure of the dispersibility of stacks, available data, illustrated by the diagram in Fig.31, suggest the relationship between the number of flakes, N_{Na}, and the salt concentration, c, that is given by Eq.12:

$$N_{Na} = 10 - 7(10^{-0.5c}) \qquad (12)$$

where c is the salt concentration in percent units.

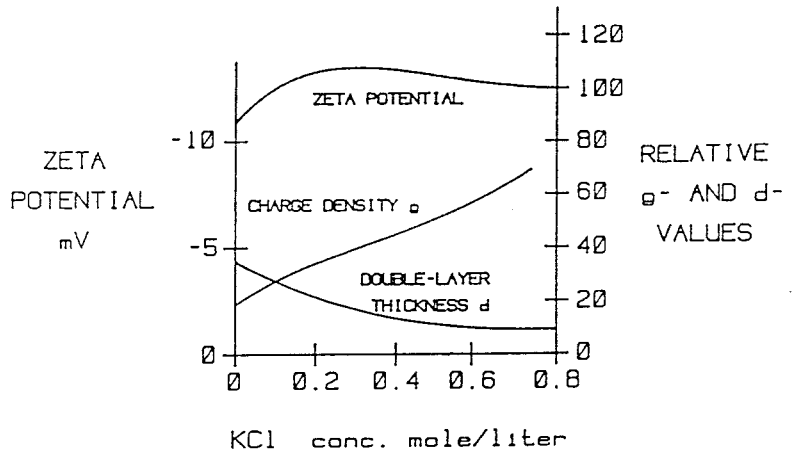

Fig.31 Example of influence of salinity on the double-layer thickness

Data derived from X-ray scattering, electron microscopy, viscosity measurements, light scattering and other data suggest that the number of flakes in Ca montmorillonite stacks is 2 to 10 times that of Na montmorillonite. Maintaining the figure 5 for Ca montmorillonite in low-saline environment, according to the basic GMM, a reasonable maximum number of flakes per stack is 15, while for lower salinities, the the number (N_{Ca}) is assumed to be given by Eq.13:

$$N_{Ca} = 15 - 10(10^{-0.5c}) \qquad (13)$$

where c is the salt concentration in percent units.

Applying the GMM we will consider again the three reference clays A,B, and C and assume that the porewater is 2 or 10 % NaCl solutions, and 2 or 10 % $CaCl_2$ solutions, respectively. As before, the expanded granules, which consist of a matrix of more or less aligned and interconnected stacks of flakes, are virtually impermeable, while the gel fillings and in certain cases unfilled parts of the "external" voids are determinants of the bulk permeability. Following the earlier appoach, the voids formed between the stacks in the gel fillings have a size that is controlled by the number of flakes per stack, and here the salt-dependent parameters N_{Na} and N_{Ca} become operative. For gels confined in very narrow "external" voids, mechanical restraints may reduce the theoretical figures in practice, but we will disregard from this in the present context.

The actual variation in aperture of continuous gel void passages is represented by a regularly varying pore geometry in the general model, the crankshaft-like shape of the passages being converted into straight capillaries with an equivalent diameter. The choice of "narrow" or "open" pore passage geometries (cf. Fig.32) does not appear to be critical and the first-mentioned option can normally be chosen. For d_1-values approaching or exceeding about 1500 Å, the "open" geometry seems more reasonable and it has also been applied in the present study with the exception of Clay A with $CaCl_2$ solution, for which the small dimensions of the "external" voids (<5 μm) still suggest the pattern with more narrow passages. For the softest Clay C with anything more salt than brackish water in its pores, the concept of "narrow" passages is not reasonable since "open" passages of the clay gels would be more or less equal to the "external" voids.

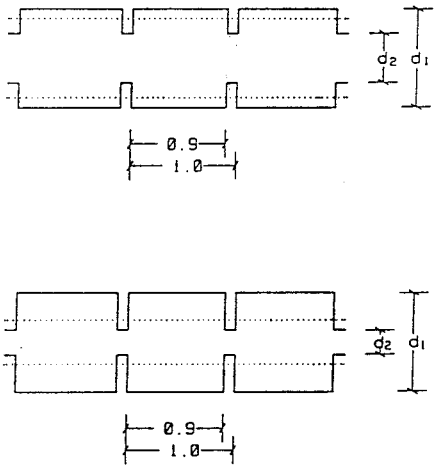

Fig.31 Geometry of schematic pore passages. Upper: "Narrow" passage characterized by an aperture $d_2=0.25\ d_1$ (length ratio $n_1=0.9$).

Lower: "Open" passage characterized by an aperture $d_2=0.5\ d_1$ (length ratio $n_1=0.9$).

As for the basic GMM, the most important parameter for the calculation of the hydraulic conductivity is the gel density since with given stack dimensions it determines the internal void space of the gels, which controls the bulk conductivity. We have applied here the same average gel densities as for the fresh-water conditions of the general model with the exception of the softest clay C, for which the conductivity has been calculated simply by assuming flow through unfilled "external" voids.

The density of the stacks forming the gels, i.e. the density of sets of flakes separated by interlamellar water, has been calculated by assuming 3 interlamellar hydrate layers in the case of NaCl porewater, and 2 interlamellar hydrates in $CaCl_2$ porewater.

The calculation of the effective porosity and quantification of the free pore space between the expanded

granules, are based on the same assumptions with respect to the number of interlamellar hydrates as the calculation of the stack density, with the exception that 2 or 3 hydrates may be developed in NaCl solutions depending on geometrical restraints at high bulk densities.

Calculation of the hydraulic conductivity of the three reference clays follows the pattern indicated in Fig.33. Applying the general model the actual tortuous system of flow passages of smectite clays is considered as sets of straight, continuous, capillary tubes, for which the Hagen-Poiseuille law can be employed to derive an expression for computing the hydraulic conductivity k. The major microstructural parameter values are given in Table 17, while Table 18 yields evaluated hydraulic conductivities together with laboratory and literature-derived data.

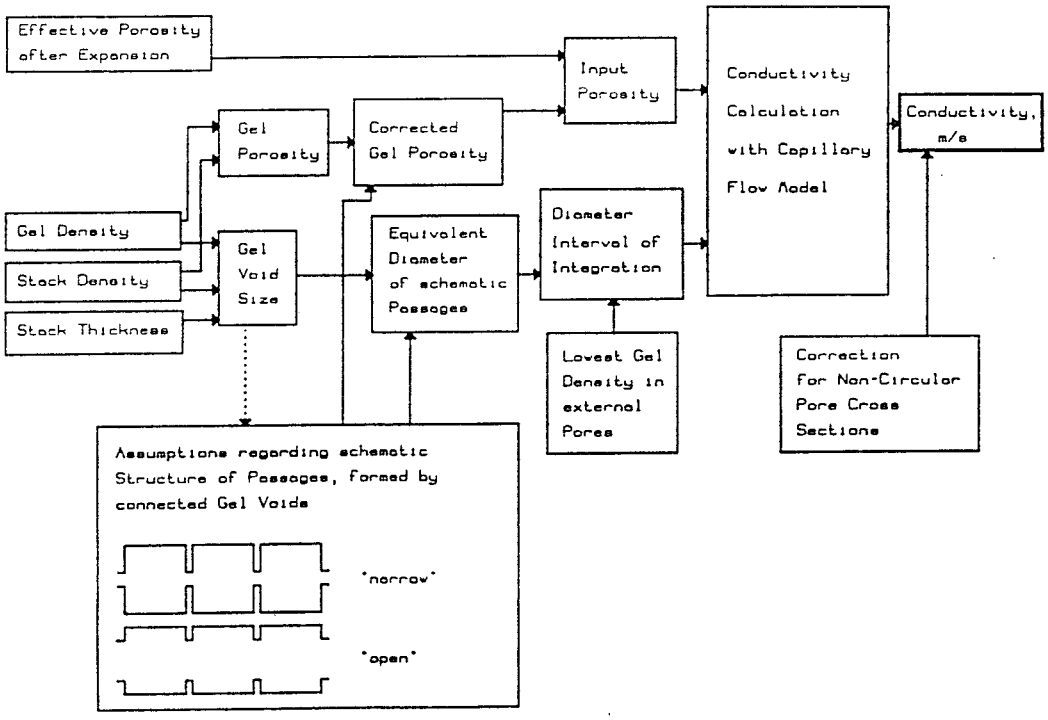

Fig.32 Flow pattern in the calculation of hydraulic conductivity at high porewater salinity

Table 17. Physical and microstructural data of refernce clays A,B, and C for various salinities; densities in g/cm^3

Clay	ρ_{sat}	Water	Minim.gel density	Flakes per st.	Stack dens.	Free sp.(Å)	Pass
A	2.13	Dist.	1.3	3	1.89	340	N*
		2% NaCl	1.3	7	1.89	860	N
		10% NaCl	1.3	10	1.89	1200	N
		2% $CaCl_2$	1.3	11	2.06	1500	N
		10% $CaCl_2$	1.3	15	2.06	2050	N
B	1.85	Dist.	1.2	3	1.89	570	N
		2% NaCl	1.2	7	1.89	1400	N/O
		10% NaCl	1.2	10	1.89	2000	O
		2% $CaCl_2$	1.2	11	2.06	2400	O
		10% $CaCl_2$	1.2	15	2.06	3300	O
C	1.57	Dist.	1.1	3	1.89	1200	N
		2% NaCl	1.0-1.05	7	1.89	**	
		10% NaCl	1.0-1.05	10	1.89	**	
		2 $CaCl_2$	1.0-1.05	11	2.06	**	
		10 $CaCl_2$	1.0-1.05	15	2.06	**	

*N=Narrow, O=Open, **Free dimensions of gel voids corresponding to size of "external" voids

Rather few systematic investigations under well defined experimental conditions appear to have been reported. The main sources, referred to in Table 18, is Nowak's report in 1981 (30) on percolation tests with very salt solutions, and comprehensive tests of Canadian bentonite holding Ca as well as Na in exchange positions. Data from Swedish investigations are sparse and no systematic tests have been made so far.

Table 18. Calculated hydraulic conductivities (k_{calc}), experimentally determined data (k_{exp}) and literature data (k_{lit}), m/s

Clay	ρ_{sat} g/cm^3	Electrolyte	k_{cal}	k_{exp}	k_{lit}
A	2.13	2% NaCl	9×10^{-14}	-	-
A	2.13	10% NaCl	10^{-13}	-	-
A	2.13	2% $CaCl_2$	2×10^{-13}	-	-
A	2.13	10% $CaCl_2$	3×10^{-13}		
	2.10	14% NaCl	2×10^{-13}	-	10^{-12}
	1.95	5% $CaCl_2$/NaCl	10^{-13}	-	10^{-13}
B	1.85	2% NaCl	2×10^{-12}	-	-
B	1.85	10% NaCl	8×10^{-12}	-	-
B	1.85	2% $CaCl_2$	5×10^{-11}	-	-
B	1.85	10% $CaCl_2$	7×10^{-11}	-	-
	1.73*	2% NaCl	2×10^{-11}	2×10^{-11}	-
	1.79*	10% NaCl	10^{-10}	4×10^{-10}	-
	1.79*	2% $CaCl_2$	10^{-9}	2×10^{-10}	-
	1.83*	10% $CaCl_2$	3×10^{-9}	2×10^{-10}	-
	1.65	5% $CaCl_2$/NaCl	10^{-10}-10^{-9}	-	10^{-10}
C	1.57	2% NaCl	10^{-9} -10^{-8}	-	-
C	1.57	10% NaCl	10^{-7} -10^{-6}	-	-
C	1.57	2% $CaCl_2$	10^{-7} -10^{-6}	-	-
C	1.57	10% $CaCl_2$	10^{-6} -10^{-5}	-	-

* Evaluated "effective" gel density for mixtures of 50/50 Mx-80 and fine quartz powder

The lack of reliable data makes it difficult to draw safe conclusions on the effect of high salinities on the conductivity and on the applicability of the flow model. However, there is reasonable agreement, i.e. less deviation than by one order of magnitude, between GMM predictions and data from the ongoing SKB study, which tends to indicate that the influence of even rather salt percolates on the hydraulic conductivity of smectite clays is small when the bulk density at saturation is higher than about 1.9 g/cm^3,

while it is very significant when the density is below about 1.7 g/cm^3.

Rough estimates of the influence of salt water on the hydraulic conductivity based on the GMM yield the following relationships between the conductivity k and the bulk density ρ_{sat} for 10 % chloride solutions:

Na montmorillonite clay:
$(1.7<\rho_{sat}<2.1$ g/cm$^3)$

$$k = 0.0125\rho_{sat}^{-33.7} \quad \text{m/s} \qquad (14)$$

Ca montmorillonite clay:
$(1.7<\rho_{sat}<2.1$ g/cm$^3)$

$$k = 13.68\rho_{sat}^{-42.3} \quad \text{m/s} \qquad (15)$$

3.2.4 *Diffusion through GMM clay*

3.2.4.1 General

Application of earlier microstructural models based on the same main idea of a heterogeneous clay matrix as the present GMM (25), has demonstrated that diffusive transport of anions is largely restricted to the "external", gel-filled voids while cation diffusion takes place much more homogeneously. Thus, it has been shown that for montmorillonite clay with a bulk density corresponding to that of the reference clay A, anion (I,Cl) diffusion capacity is only a few percent of that of cations (Cs,Sr), and that the anion diffusion capacity appears to be proportional to the "effective" porosity, i.e. the ratio of the "external" voids after maturation, and the total volume (31). This supports the idea that anions are prevented from entering the interlamellar space by Donnan exclusion, and that the microstructural pattern of the GMM is correct in principle.

As to cation diffusion, it is expected that it takes place in several ways, which can be described as pore diffusion and surface diffusion. The latter has the

form of both diffusion along basal planes of stacks and diffusion through interlamellar space, and it is reasonable to believe that the first-mentioned type of migration takes place rather quickly in the assumed low-viscous water layer (B in Fig.12). Interlamellar diffusion, on the other hand, at least partly involves cation exchange, which requires that energy barriers must be overcome. At interlamellar diffusion of calcium or copper through initially sodium saturated clay, the replacement of sodium ions by bivalent cations presumably requires breakage of strong hydrogen bonds, since collapse of the assumed water lattice would take place before the bivalent cations become established in hydrated form.

Consequently, sodium would be expected to diffuse with less resistance in the interlamellar space, yielding both a high diffusion rate and capacity. Due to the tortuosity of the passages in montmorillonite clay the diffusivity can of course not be as high as in bulk water, i.e. about 1.5×10^{-9} m^2/s, but one would expect a diffusion coefficient of around 10 times this figure and this is also what carefully conducted tests actually yield, namely about 2×10^{-10} m^2/s for clay of type A (32). Of even greater interest is that the bulk density of the clay is of no particular importance. Thus, it is expected that since diffusion takes place both through voids and stacks as well as along stacks, it would be characterized by approximately the same rate coefficient almost irrespective of the bulk density. This is validated by the fact that the apparent coefficient of diffusion of sodium through Na montmorillonite clay with a density similar to that of the soft reference clay C is 3×10^{-10} m^2/s.

Considering diffusion of copper, which has been investigated in long-term experiments, the conditions are more complex since precipitation processes may take place and cause difficulties in the evaluation of relevant diffusion parameters (32). It is concluded from

such tests that the apparent coefficient of diffusion is higher for higher densities, i.e. $3x10^{-11}$ m^2/s for clays similar to Clay A and $7x10^{-12}$ m^2/s for a clay with slightly lower density than that of Clay C, and that it is appreciably lower than for sodium. The latter fact suggests that copper almost entirely migrates along and through stacks, the latter process being hindered by the afore-mentioned ion exchange process. The rate-enhancing effect of the density is logically explained by the much better continuity of the stack network in denser clays.

A major conclusion is that the GMM seems to offer a basis for qualitative understanding of the mechanisms involved in anion and cation diffusion and also for quantitative estimation of ion diffusion capacity. Quantitative predictions of the diffusion capacity of various species are possible using the GMM but validation requires systematic tests under conditions that eliminate precipitation and chemical reactions between the solutes and the minerals. Further comments are given in a later chapter on effects of heating on the microstructure and transport mechanisms.

3.2.5 *Swelling pressure in GMM clay*

3.2.5.1 Microstructural implications

Theoretically, the swelling pressure of the presently discussed artificially produced clays can be deduced by integrating the repulsive forces over a cross section through the clay, considering the pressure between adjacent flakes in the stacks as well as the double-layer repulsion caused by electric charges and "disjoining" pressure. In practice, such derivations would not yield very accurate figures because the number of flakes in the stacks varies depending on the stress distribution

and since the contribution from overlapping electrical double-layers is a function of the varying distance between adjacent stacks (Fig.33).

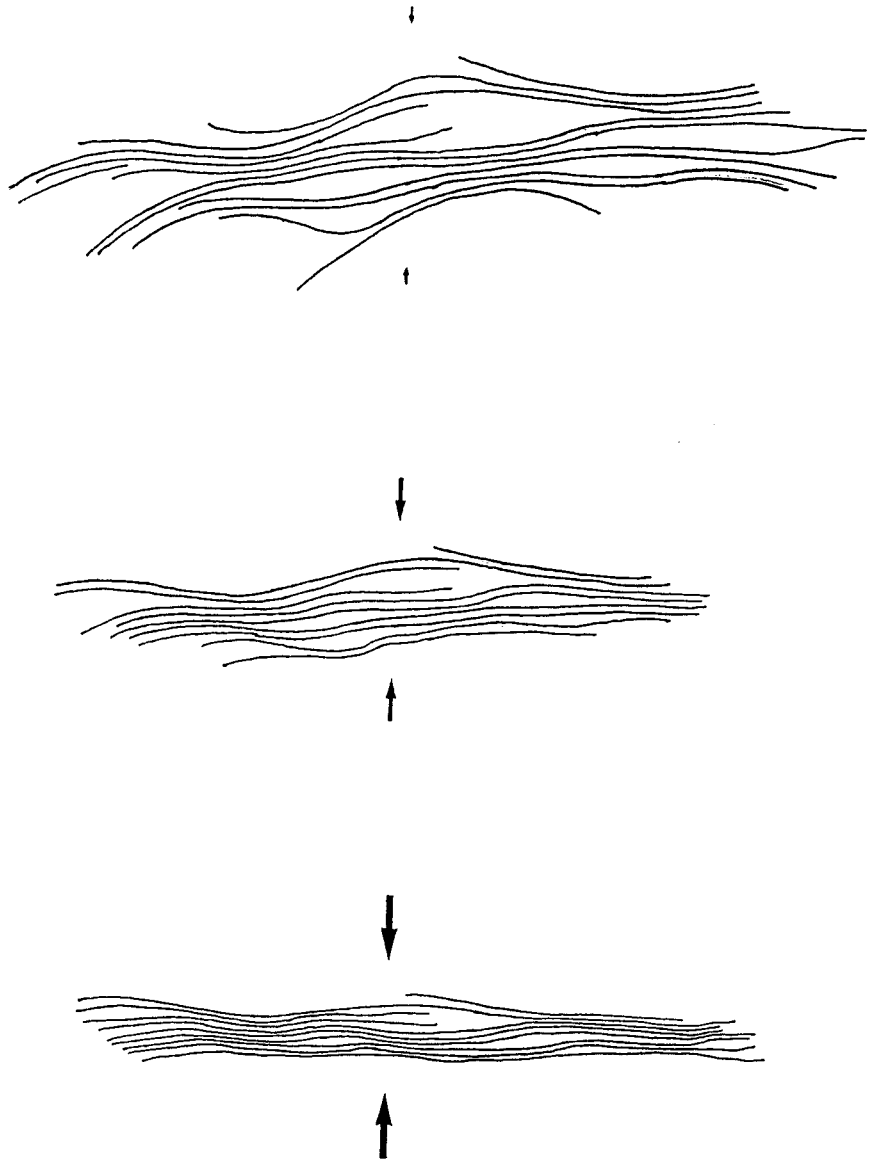

Fig.33 Schematic picture of stacks of montmorillonite flakes indicating a change from fully hydrated state with 3 hydrates (upper) to 1-3 hydrates (lower) and corresponding variations in distance between stacks

At best, qualitative estimates of the swelling pressure can be made and this requires that the earlier mentioned influence of the kind and concentration of dissolved cations in the porewater is taken into consideration in addition to the density, which is of fundamental importance.

3.2.5.2 Influence of density and electrolytes on the swelling pressure

For Na montmorillonite the maximum number of interlamellar hydrates is 3, which means that a fully expanded state of the stacks is theoretically obtained at around 1.8 g/cm^3, while the corresponding figure for Ca montmorillonite, or more generally montmorillonite saturated with bivalent cations, is slightly lower. This means that below these critical densities, the swelling pressure is entirely controlled by electrical double-layer repulsion.

Since the number of stack contacts and therefore also of interacting electrical double-layers is much larger in Na montmorillonite than in montmorillonite saturated with bivalent cations, one would expect a stronger influence of cation concentration in Na montmorillonite. This means, in turn, that the swelling pressure for densities below the critical levels should be very low at almost any salinity in Ca montmorillonite and at high Na concentrations in Na montmorillonite, while it should increase from a very low value to an appreciable pressure in Na montmorillonite with with very low ionic strength when its density increases from a low value to the critical level. This would suggest the schematic relationships between density, cation concentration and swelling pressure indicated in Figs.34-36.

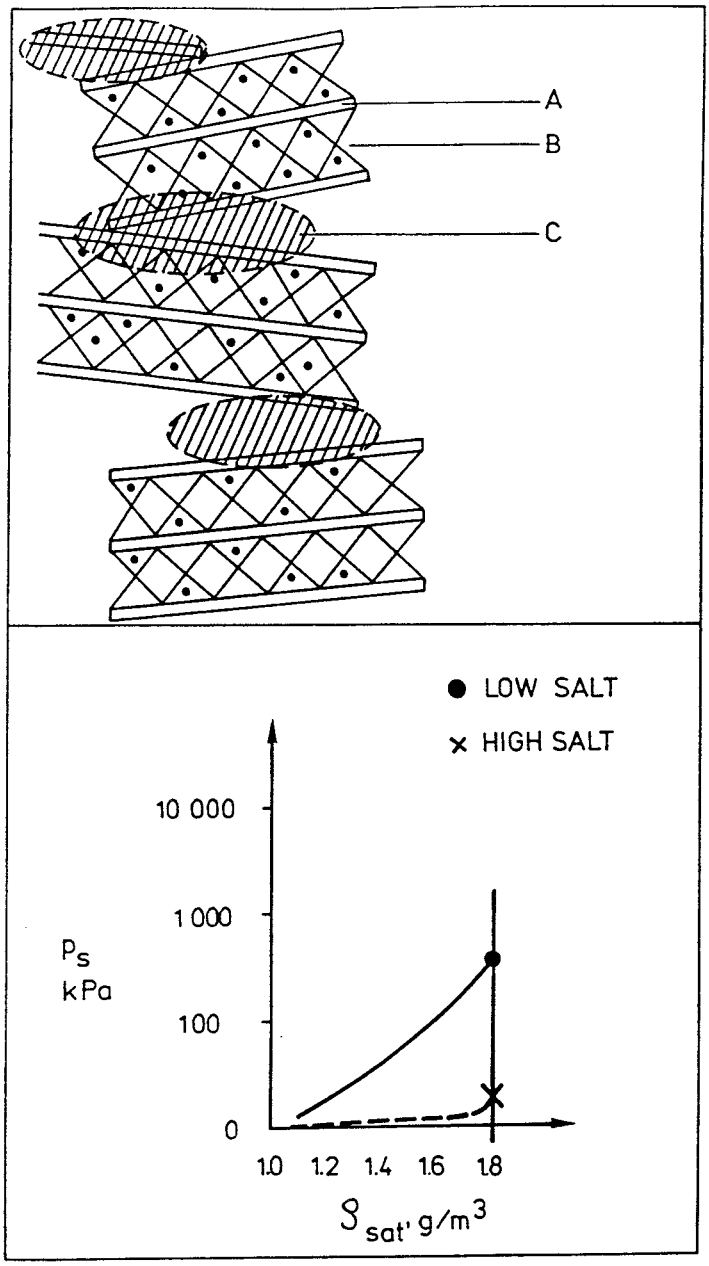

Fig.34 Schematic picture of the stack assemblage in Na montmorillonite and influence of ion strength on the swelling pressure at low densities. A) montmorillonite flake, B) interlamellar space, C) stack contact with interacting electrical double-layers and "disjoining" water

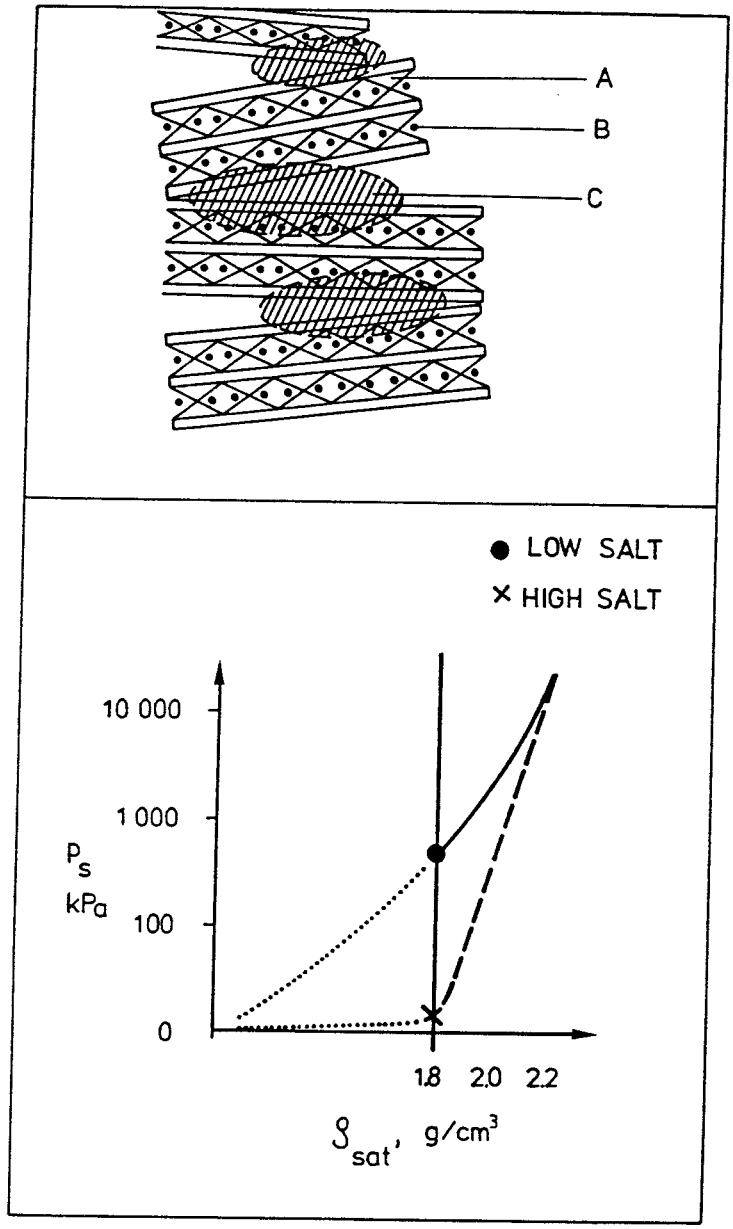

Fig.35 Same as Fig.34 at high densities

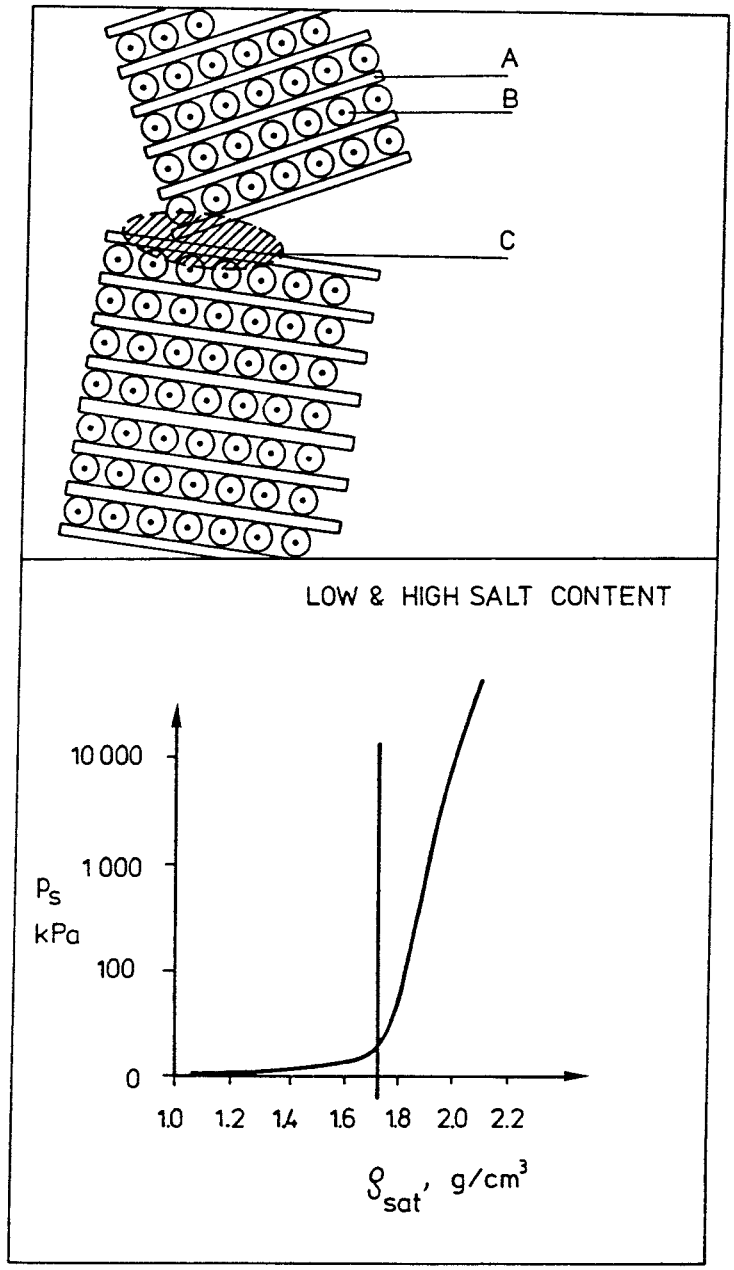

Fig.36 Schematic picture of stack assemblage in Ca montmorillonite and influence of density and salinity on the swelling pressure. (Legend as in Fig.34)

Recordings of the swelling pressure, which turns out to be somewhat dependent on whether it is measured under compression or expansion, are in very good agreement with data generated by the models derived here for low ionic strengths (Fig.37). Ongoing studies at high ionic strength tend to support the models as well. Thus, one finds the approximate relationsship between swelling pressure and density at saturation that is shown in Table 19 to be in satisfactory agreement with the predictions in Figs.34-36. Hence, the GMM verifies, in principle, the assumed internal force fields in montmorillonite clays of different densities at room temperature and different salinities.

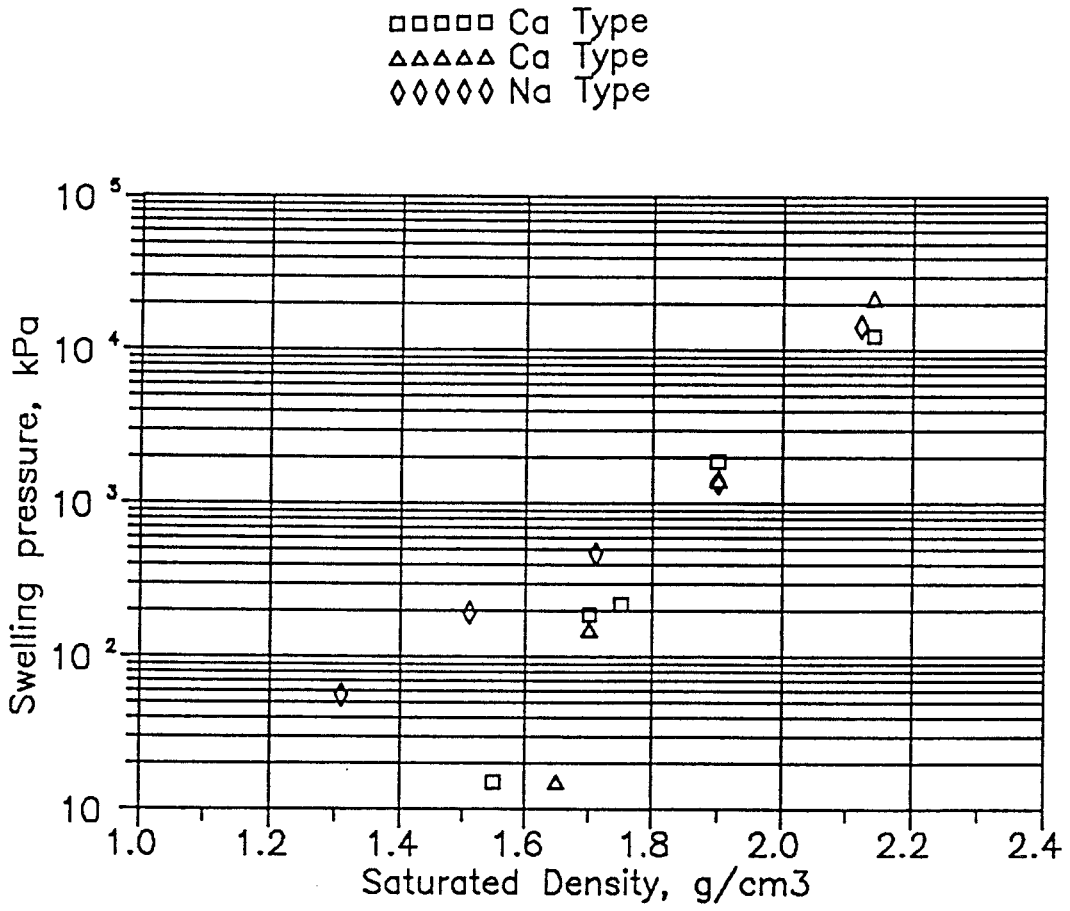

Fig.37 Recorded swelling pressures of Na and Ca montmorillonite clays saturated with distilled water

Table 19. Preliminary swelling pressure data from oedometer tests with highly saline clays

Density at saturation, g/cm^3	Pore water	Swelling press. MPa
1.73*	2 % NaCl	0.29
1.79*	10 % NaCl	0.27
1.80*	2 % $CaCl_2$	0.65
1.83*	10 % $CaCl_2$	1.20

* Evaluated "effective" gel density for mixtures of 50/50 MX-80 and fine quartz powder

3.2.6 *Critical gas pressure*

The critical gas pressure concept is based on the experimental fact that gas does not penetrate clay until a certain pressure level is reached, as well as on capillary analogy (25). Putting together the main microstructural data of the GMM reference clays, we see that the actually measured critical gas pressure is on the same magnitude as those predicted by applying capillary analogies for the densest clay A (Table 20). This means that the voids of the gel fillings control the critical pressure with only slight consolidation of the gels, at which the swelling pressure of the clay begins to be mobilized.

For Clay B we find that the capillary analogy yields a significantly higher critical pressure than was actually recorded, which may be explained by consolidation of the soft gels in the widest voids by which channels with a diameter of around 0.2 μm were formed. The increase in gel density produced by such consolidation is assumed to generate a slight swelling pressure that is sufficient to partly close the channel at a temporary drop in gas pressure. This will stop the gas flow and

require a pressure increase to approximately the initial critical pressure before gas penetration starts again, as has also been found experimentally. However, it is not known if this behavior is preserved at long-term gas percolation.

Table 20. Measured and predicted critical gas pressures of reference clays A,B, and C in sodium form

Clay	Ext.void diam. μm	Gel void diam. μm	Crit. gas.pr. MPa	
			Predict.	Meas.
A	1-5	0.015	20	21
B	1-20	0.025	10	1.5
C	1-50	0.050	6	0.4

For Clay C gas penetration will certainly produce consolidation of the gel fillings in the widest external voids, by which channnels with about 1 μm aperture become formed according to the model.

The very low frequency of wide external voids would suggest that gas penetrates dense smectite clays in only a very small number of passages. One would assume that gas-pressurized clays of type A and B let gas through passages that have a spacing of 100 -1000 μm and this is in reasonable agreement both with the GMM and with actual observations (33).

3.3 Heat effects on GMM clay

3.3.1 *General*

The influence of heating on smectite has been the issue

of a number of studies, primarily with the aim of relating temperature to the chemical stability of smectite minerals. We will confine ourselves here to consider physical processes only, disregarding from dissolution, precipitation and crystal lattice alteration of the minerals.

3.3.2 *Influence of heating on conductivity and swelling pressure of Na montmorillonite*

Starting with Na montmorillonite and applying the idea of interlamellar water lattices established in the interlamellar space, one would expect, from thermodynamic points of view, that significantly increased thermal vibrations would yield instability of the interlamellar hydrates. Thus, under the influence of a constant effective pressure the number of hydrates would be reduced *locally where stress transfer between the stacks takes place so that the intial spectrum of hydrate numbers will change to yield more 1-hydrate "contacts", which are not assumed to be sensitive to temperatures below 100-120^{o}C or pressures lower than at least 100 MPa.* 1-hydrate interlamellar contacts dominate already at bulk densities at saturation of about 2 g/cm^{3}.

The large majority of the interlamellar space both in the stacks of the expanded granules and in the gel fillings would remain unaffected at any bulk density and even at relatively low densities the change in "external" void size is also expected to be very small. Hence, the average hydraulic conductivity is not expected to undergo much change by heating; it may be a matter of some slight decrease but in practice it is expected to be controlled by the thermal increase in water viscosity. Thus, heating to 90 or 130^{o}C is expected to increase the conductivity by 3 and 5 times, respectively.

The increased double-layer repulsion of adjacent stacks, which is analogous to the heat-induced increase in osmotic pressure in any ionic or molecular system, would require a raise in applied pressure to maintain constant volume at densities lower than the critical level, i.e. about 1.8 g/cm^3, while practically no increase in pressure would be required at high densities since double-layer repulsion adds very little to the swelling pressure above 1.9-2.0 g/cm^3. On cooling back to room temperature, rehydration of the contracted parts of contacting stacks takes place, by which the stress transferred by them is somewhat reduced, and since the double-layer repulsion is also reduced, one would expect a reduction in swelling pressure back to approximately the original value. The less effective double-layer repulsion caused by salt water at any given clay density would suggest that the heat-induced increase in swelling pressure is negligible. Likewise, the net change in hydraulic conductivity by a heating/-cooling cycle is expected to be negligible.

Table 21, which refers to oedometer tests with constant volume, supports the predicted behavior with respect to the hydraulic conductivity. Thus, we see that for Na montmorillonite the average conductivity increased by about 2 times when the temperature was raised from room temperature to 90^{o}C, and by around 3 times when heating took place to 130^{o}C, indicating very slight microstructural changes in the course of the heating cycle. A somewhat higher increase, corresponding almost entirely to the change in water viscosity, was found for the salt porewaters.

Table 22 shows swelling pressures measured in the oedometer after complete porewater dissipation and one finds that the data in good qualitative agreement with the predictions. Thus, there is an increase by about 50 % of the swelling pressure for bulk densities of around 1.8 g/cm^3 using distilled water, while there is hardly

any change at higher densities. For salt porewater, there is no change in swelling pressure at all.

Table 21. Hydraulic conductivity of Na montmorillonite clay at high temperatures; the figures must be multiplied by 10^{-13} to yield k in m/s

Density at saturation g/cm^3	Water	Temperature, °C				
		20	90	130	90	20
1.61	Dist.	71	170	230	140	42
1.81	Dist.	11	21	35	18	9
2.00	Dist.	2	4	6	3	1
2.06	Dist.	1	2	3	2	0.6
1.73*	2% NaCl	200	1100	1100	1100	360
1.79*	10% NaCl	4000	16000	19000	16000	4700

* Evaluated "effective" gel density for mixtures of 50/50 MX-80 and fine quartz powder

Table 22. Swelling pressure of Na montmorillonite at high temperatures, MPa

Density at saturation g/cm^3	Water	Temperature, °C				
		20	90	130	90	20
1.61	Dist.	0.12	0.17	0.20	0.18	0.12
1.80	Dist.	0.72	1.04	-	-	0.71
2.00	Dist.	4.66	5.68	-	-	4.83
2.06	Dist.	9.25	9.00	8.89	8.05	8.40
1.73*	2% NaCl	0.25	0.25	0.26	0.26	0.29
1.79*	10% NaCl	0.28	0.28	0.27	0.26	0.27

* Evaluated "effective" gel density for mixtures of 50/50 MX-80 and fine quartz powder

3.3.3 *Influence of heating on conductivity and swelling pressure on Ca montmorillonite*

The strong hydration power of calcium ions means that there are two hydrates in the interlamellar space even at bulk densities at saturation of about 2 g/cm^3 at room temperature, while the number of hydrates is only 1 in Na montmorillonite stacks where the major part of stress transfer takes place in interacting stacks. Like in Na montmorillonite, heating will produce an unstable hydration state and this means that even a relatively moderate increase in temperature is expected to cause a reduction of the number of hydrates. Hence, a reduction from 2 hydrates to 1 is expected to take place in large parts of many stacks, leading to a reduction in swelling pressure.

The fact that the number of flakes per stack is considerably higher in Ca than in Na montmorillonite clay means that the amount of electrical double-layers per unit volume is significantly smaller in the first-mentioned type of clay, which suggests that the heat-induced raise in "osmotic" pressure is less important than in Na montmorillonite. The two counteracting effects are therefore expected to yield a net reduction in swelling pressure and this is also confirmed by test results shown in Table 23. The fact that the drop in swelling pressure is particularly strong in Ca montmorillonite clay with a high ionic strength indicates that double-layer interaction still makes an important contribution to the swelling pressure at low and medium densities as implied by the GMM.

The microstructural changes associated with heating are expected to be more obvious than for Na montmorillonite but current tests indicate that the influence of heating to 130^{o}C gives approximately the same change in hydraulic conductivity as for sodium clay. *This leads us to believe that heating of clay formed by water saturated granular bentonite powder has*

a homogenizing effect by thermomechanically induced breakage of cementing bonds that are inherited from the natural bentonite beds.

Table 23. Swelling pressure of Ca montmorillonite at high temperatures, MPa

Density at saturation g/cm^3	Water	Temperature, °C				
		20	90	130	90	20
1.67	Dist.	0.25	-	-	-	-
2.00	Dist.	9.0	7.5	7.0	6.5	7.8
1.79*	2% $CaCl_2$	0.71	0.66	0.53	0.50	0.63
1.83*	10% $CaCl_2$	1.31	0.79	0.64	0.59	1.17

* Evaluated "effective" gel density for mixtures of 50/50 MX-80 and quartz powder

3.3.4 *Conclusive remarks on the influence of heating respecting the validity of GMM model*

Qualitatively, the GMM is in good agreement with actually recorded changes in physical properties of montmorillonite clay. It must be kept in mind, however, that chemical effects become important when the temperature is raised beyond 50-60°C, which means that long-term measurements may be strongly affected by chemically induced changes.

Also, the conditions under which heating is performed is very essential. Thus, heating under closed conditions will raise the pore pressure to very high values, which, according to the model, will drive "interstitial" water molecules into the interlamellar space and this may create unstable stress conditions resulting in disintegration of stacks, while subsequent cooling may yield the reverse. The net effect would still be an improved degree of homogeneity but the ori-

ginal relationship between "internal" and "external" water may not be obtained. Theoretically, at least, disintegration of stacks due to exposure to heat or to intense mechanical agitation, as in heavy compaction, may result in almost complete separation into individual flakes that may not be spontaneously reorganized to form stacks, and this may strongly reduce the amount of "organized" interlamellar water and thereby the swelling ability of Na montmorillonite.

4 COMMENTS AND GENERAL CONCLUSIONS

The presently proposed microstructural model with the assumed force-fields on the molecular scale appears to form a basis for qualitative understanding of a number of experimentally recorded changes in physical properties on altering the density and the porewater electrolytes, as well as on heating. It is concluded also, that it can be used for prediction of the transport capacity of water and of dissolved ions under gradients that may be induced in clays used as buffers and backfillings in reporitories. *It is of particular interest to see that its inherent character would allow for an extension to account also for chemically induced changes, such as dissolution/neoformation, mixed-layer formation, and precipitation of cementing substances involved in hydrothermal treatment at high temperatures. Such extension is strongly recommended since it would yield a model that, after calibration using natural analogues ("illitization" etc), can be directly used in the outlining of scenarios of the respective radwaste concepts.*

In conjunction with the study of the GMM and the comparison between predicted and experimentally obtained data a number of important facts were found, the major ones being:

1. The hydraulic conductivity of Na montmorillonite clay is only slightly affected by even very significantly increased salinities with Na or Ca as major adsorbed cation at higher bulk densities than about 1.8 g/cm^3. At lower densities the increase in conductivity of Na montmorillonite is significant but even at densities corresponding to that of grouts, the conductivity is still low as compared to non-smectitic clays in nature.

2. Ca montmorillonite clay formed from Ca bentonite granules is not coherent and becomes extremely pervious at lower densities than about 1.5 g/cm^3 when the salinity is raised to the level that prevails at large depths in granitic bedrock. At higher density than about 1.8 g/cm^3, the hydraulic conductivity is only moderately altered even at very high porewater salinities with Ca as major cation

3. Heating actually *reduces* the true conductivity, i.e. disregarding from the heat-induced drop in water viscosity irrespective of whether sodium or calcium are in exchange positions or whether the ion strength is high or low

4. Heating actually *increases* the swelling pressure of Na montmorillonite even at high salinity except for high densities, i.e. about 2 g/cm^3 where no change takes place. For Ca montmorillonite the swelling pressure *decreases* by 25 to 50 % on heating, the salinity being of small importance

5 REFERENCES

1. Forslind,E. The Clay-Water System. Bull. No 11, Swedish Cement and Concrete Research Inst., 1948

2. Sposito,G. The Surface Chemistry of Soils. Oxford Univ. Press, Oxford 1984

3. Tardy,Y. & Touret,O. A Method of Estimating Gibbs Free Energies of Formation of Hydrated and Dehydrated Clay MInerals. Int. Rep. Centre de Sedimentologie et de Geochimie de la Surface, Strasbourg, 1988

4. Pusch,R. & Karnland,O. Aspects of the Physical State of Smectite-adsorbed Water. SKB Technical Report 86-25, 1986

5. Pinnavaia,T.J., Landau,S.D., Tzou,M-S & Johnson,I.D. Layer Cross Linking in Pillared Clays. J. Am. Chem. Soc. Vol. 107, 1985 (pp.7223-7224)

6. Woessner,D.E. & Snowden,B.S. A Study of Adsorbed Water Molecules on Montmorillonite Clays by Pulsed NMR. J. Colloid and Interface Science, Vol.30, No.1 1969

7. Drost-Hansen,W. Water Near Solid Interfaces. Industrial and Engineering Chemistry. Vol.61, No.11, 1969 (pp.10-47)

8. Yong,R. & Warkentin,B.P. Soil Properties and Behaviour. Elsevier Publ Co., 1975

9. Pusch,R. Engineering Aspects of Clay-weathered Blekinge Gneiss. Geol. Fören. i Sthlm Förh. Vol.101, Pt 1, 1979 (pp.27-31)

10. Derjaguin,B.V. % Obuchev,E. Anomalien dunner Flussigkeitsschichten, III. Acta Physicochimica U.R.S.S., Vol.V, No.1, 1936 (pp.1-21)

11. Frenkel,J. Kinetic Theory of Liquids. Oxford University Press, Oxford, 1946

12. Low,P.F. Nature and Properties of Water in Montmorillonite-Water Systems. Soil Science Soc. Am. J. Vol.45, 1979 (p.651)

13. Low,P.F. The Swelling of Clay III. Dissociation of Exchangeable Cations. Reprint of Journal Paper, Agronomy Dep. Purdue University, Agricultural Experiment Station, West Lafayette, Indiana, 1980

14. Derjaguin,B.V. & Churaev,N.W. Structural Component of Disjoining Pressure. J. Colloid and Interface Science. Vol.48, 1974 (pp.249-255)

15. Israelachvili,J.N. & Adams,G.E. Measurement of Forces Between Two Mica Surfaces in Aqueous Electrolyte Solutions in the Range 0-100 nm. J. Chem. Soc. Faraday Trans. I, Vol.74, 1978 (pp.975-1001)

16. Woessner,D.E. An NMR Investigation Into the Ranges of the Surface Effect on the Rotation of Water Molecules. J. Magn. Res., Vol.39, 1980

17. Carlsson,T. Interactions in MX-80 Bentonite/ Water/Electrolyte Systems. Doct. Thesis 1986:55 D, University of Luleå, 1986

18. Börgesson,L.& Pusch,R. Rheological Properties of a Calcium Smectite. SKB Technical Report 87-31, 1987

19. Börgesson,L., Hökmark,H., Karnland,O. Rheological Properties of Sodium Smectite Clay. SKB Technical Report 88-30, 1988

20. Mitchell,J.K. Shearing Resistance as a Rate Process. J. Soil Mech. a Found. Div. ASCE, Vol.90, No SM1, 1964 (pp.29-61)

21. Kuhn,M.R. Micromechanical Aspects of Soil Creep. Diss. Univ. of California, Berkeley, 1987

22. Feltham,P. A Simple Stochastic Model of Low-temperature Creep and Stress-Relaxation in Solids. Proc. VII Int. Congr. on Rheology. Chalmers Techn. Univ. Gothenburg 1976

23. Pusch,R. & Feltham,P. A Stochastic Model of the Creep of Soils. Geotechnique, Vol.30, No.4, 1980 (pp.497-506)

24. Pusch,R., Börgesson,L., Erlström,M. Alteration of Isolating Properties of Dense Smectite Clay in Repository Environment as Examplified by Seven Pre-Quaternary Clays. SKB Technical Report 87-29, 1987

25. Pusch,R. & Hökmark,H. Outline of Models of Water and Gas Flow Through Smectite Clay Buffers. SKB Technical Report 87-10, 1987

26. Athanasiou-Grivas,D. & Harr,M.E. The Path of Flow and Its Effect on Consolidation Rates. 3rd Int. Conf. on Numerical Methods in Geomechanics, Aachen 1979, W.Wittke (Ed). Balkema, Rotterdam, 1979

27. Pusch,R. Identification of Na-Smectite Hydration by Use of "Humid Cell" High Voltage Microscopy. Appl. Clay Sci. Vol.2 1987 (pp.343-352)

28 Bryant,W.R. & Bennett,R.H. Origin, Physical, and Mineralogical Nature of Red Clays: The Pacific Ocean Basin as a Model. Geo-Marine Letters. Vol.8, 1988 (pp.189-249)

29. Tessier,D. & Pedro,G. Electron Microscopy Study of Na Smectite Fabric - Role of Layer Charge, Salt Concentration and Suction Parameters. Developments in Sedimentology, Vol.35, Int. Clay Conference 1981, Elsevier Publ. Co.

30. Nowak,E.J. Composite Backfill Materials for Radioactive Waste Isolation by Deep Burial in Salt. Scientific Basis for Nuclear Waste Management. Ed. John G. Moore, Vol.3, Plenum Press, 1981 (pp. 545 - 552)

31. Pusch,R. & Carlsson.T. The Physical State of Pore Water of Na Smectite Used as Barrier Component. Engineering Geology, Vol.21, 1985 (pp.257-265)

32. Pusch,R., Karnland,O., & Muurinen,A. Transport and Microstructural Phenomena in Bentonite Clay With Respect to the Behavior and Influence of Na, Cu, and U. SKB Technical Report 89-34, 1989

33. Pusch,R., Ranhagen,L., & Nilsson,K. Gas Migration Through MX-80 Bentonite. NAGRA Technical Report 85-36, 1985

List of SKB reports

Annual Reports

1977-78
TR 121
KBS Technical Reports 1 – 120
Summaries
Stockholm, May 1979

1979
TR 79-28
The KBS Annual Report 1979
KBS Technical Reports 79-01 – 79-27
Summaries
Stockholm, March 1980

1980
TR 80-26
The KBS Annual Report 1980
KBS Technical Reports 80-01 – 80-25
Summaries
Stockholm, March 1981

1981
TR 81-17
The KBS Annual Report 1981
KBS Technical Reports 81-01 – 81-16
Summaries
Stockholm, April 1982

1982
TR 82-28
The KBS Annual Report 1982
KBS Technical Reports 82-01 – 82-27
Summaries
Stockholm, July 1983

1983
TR 83-77
The KBS Annual Report 1983
KBS Technical Reports 83-01 – 83-76
Summaries
Stockholm, June 1984

1984
TR 85-01
Annual Research and Development Report 1984
Including Summaries of Technical Reports Issued during 1984. (Technical Reports 84-01 – 84-19)
Stockholm, June 1985

1985
TR 85-20
Annual Research and Development Report 1985
Including Summaries of Technical Reports Issued during 1985. (Technical Reports 85-01 – 85-19)
Stockholm, May 1986

1986
TR 86-31
SKB Annual Report 1986
Including Summaries of Technical Reports Issued during 1986
Stockholm, May 1987

1987
TR 87-33
SKB Annual Report 1987
Including Summaries of Technical Reports Issued during 1987
Stockholm, May 1988

1988
TR 88-32
SKB Annual Report 1988
Including Summaries of Technical Reports Issued during 1988
Stockholm, May 1989

1989
TR 89-40
SKB Annual Report 1989
Including Summaries of Technical Reports Issued during 1989
Stockholm, May 1990

Technical Reports
List of SKB Technical Reports 1990

TR 90-01
FARF31 –
A far field radionuclide migration code for use with the PROPER package
Sven Norman[1], Nils Kjellbert[2]
[1]Starprog AB
[2]SKB AB
January 1990

TR 90-02
Source terms, isolation and radiological consequences of carbon-14 waste in the Swedish SFR repository
Rolf Hesböl, Ignasi Puigdomenech, Sverker Evans
Studsvik Nuclear
January 1990

TR 90-03
Uncertainties in repository performance from spatial variability of hydraulic conductivities –
Statistical estimation and stochastic simulation using PROPER
Lars Lovius[1], Sven Norman[1], Nils Kjellbert[2]
[1]Starprog AB
[2]SKB AB
February 1990

TR 90-04
Examination of the surface deposit on an irradiated PWR fuel specimen subjected to corrosion in deionized water
R. S. Forsyth, U-B. Eklund, O. Mattsson, D. Schrire
Studsvik Nuclear
March 1990

TR 90-05
Potential effects of bacteria on radionuclide transport from a Swedish high level nuclear waste repository
Karsten Pedersen
University of Gothenburg, Department of General and Marine Microbiology, Gothenburg
January 1990

TR 90-06
Transport of actinides and Tc through a bentonite backfill containing small quantities of iron, copper or minerals in inert atmosphere
Yngve Albinsson, Birgit Sätmark,
Ingemar Engkvist, W. Johansson
Department of Nuclear Chemistry,
Chalmers University of Technology, Gothenburg
April 1990

TR 90-07
Examination of reaction products on the surface of UO_2 fuel exposed to reactor coolant water during power operation
R. S. Forsyth, T. J. Jonsson, O. Mattsson
Studsvik Nuclear
March 1990

TR 90-08
Radiolytically induced oxidative dissolution of spent nuclear fuel
Lars Werme[1], Patrik Sellin[1], Roy Forsyth[2]
[1]Swedish Nuclear Fuel and waste Management Co (SKB)
[2]Studsvik Nuclear
May 1990

TR 90-09
Individual radiation doses from unit releases of long lived radionuclides
Ulla Bergström, Sture Nordlinder
Studsvik Nuclear
April 1990

TR 90-10
Outline of regional geology, mineralogy and geochemistry, Poços de Caldas, Minas Gerais, Brazil
H. D. Schorscher[1], M. E. Shea[2]
[1]University of Sao Paulo
[2]Battelle, Chicago
December 1990

TR 90-11
Mineralogy, petrology and geochemistry of the Poços de Caldas analogue study sites, Minas Gerais, Brazil
I: Osamu Utsumi uranium mine
N. Waber[1], H. D. Schorscher[2], A. B. MacKenzie[3], T. Peters[1]
[1]University of Bern
[2]University of Sao Paulo
[3]Scottish Universities Research & Reactor Centre (SURRC), Glasgow
December 1990

TR 90-12
Mineralogy, petrology and geochemistry of the Poços de Caldas analogue study sites, Minas Gerais, Brazil
II: Morro do Ferro
N. Waber
University of Bern
December 1990

TR 90-13
Isotopic geochemical characterisation of selected nepheline syenites and phonolites from the Poços de Caldas alkaline complex, Minas Gerais, Brazil
M. E. Shea
Battelle, Chicago
December 1990

TR 90-14
Geomorphological and hydrogeological features of the Poços de Caldas caldera, and the Osamu Utsumi mine and Morro do Ferro analogue study sites, Brazil
D. C. Holmes[1], A. E. Pitty[2], R. Noy[1]
[1]British Geological Survey, Keyworth
[2]INTERRA/ECL, Leicestershire, UK
December 1990

TR 90-15
Chemical and isotopic composition of groundwaters and their seasonal variability at the Osamu Utsumi and Morro do Ferro analogue study sites, Poços de Caldas, Brazil
D. K. Nordstrom[1], J. A. T. Smellie[2], M. Wolf[3]
[1]US Geological Survey, Menlo Park
[2]Conterra AB, Uppsala
[3]Gesellschaft für Strahlen- und Umweltforschung (GSF), Munich
December 1990

TR 90-16
Natural radionuclide and stable element studies of rock samples from the Osamu Utsumi mine and Morro do Ferro analogue study sites, Poços de Caldas, Brazil
A. B. MacKenzie[1], P. Linsalata[2], N. Miekeley[3], J. K. Osmond[4], D. B. Curtis[5]
[1]Scottish Universities Research & Reactor Centre (SURRC), Glasgow
[2]New York Medical Centre
[3]Catholic University of Rio de Janeiro (PUC)
[4]Florida State University
[5]Los Alamos National Laboratory
December 1990

TR 90-17
Natural series nuclide and rare earth element geochemistry of waters from the Osamu Utsumi mine and Morro do Ferro analogue study sites, Poços de Caldas, Brazil
N. Miekeley[1], O. Coutinho de Jesus[1], C-L Porto da Silveira[1], P. Linsalata[2], J. N. Andrews[3], J. K. Osmond[4]
[1]Catholic University of Rio de Janeiro (PUC)
[2]New York Medical Centre
[3]University of Bath
[4]Florida State University
December 1990

TR 90-18
Chemical and physical characterisation of suspended particles and colloids in waters from the Osamu Utsumi mine and Morro do Ferro analogue study sites, Poços de Caldas, Brazil
N. Miekeley[1], O. Coutinho de Jesus[1], C-L Porto da Silveira[1], C. Degueldre[2]
[1]Catholic University of Rio de Janeiro (PUC)
[2]PSI, Villingen, Switzerland
December 1990

TR 90-19
Microbiological analysis at the Osamu Utsumi mine and Morro do Ferro analogue study sites, Poços de Caldas, Brazil
J. West[1], A. Vialta[2], I. G. McKinley[3]
[1]British Geological Survey, Keyworth
[2]Uranio do Brasil, Poços de Caldas
[3]NAGRA, Baden, Switzerland
December 1990

TR 90-20
Testing of geochemical models in the Poços de Caldas analogue study
J. Bruno[1], J. E. Cross[2], J. Eikenberg[3], I. G. McKinley[4], D. Read[5], A. Sandino[1], P. Sellin[6]
[1]Royal Institute of Technology (KTH), Stockholm
[2]AERE, Harwell, UK
[3]PSI, Villingen, Switzerland
[4]NAGRA, Baden, Switzerland
[5]Atkins, ES, Epsom, UK
[6]Swedish Nuclear and Waste Management Co (SKB), Stockholm
December 1990

TR 90-21
Testing models of redox front migration and geochemistry at the Osamu Utsumi mine and Morro do Ferro analogue sites, Poços de Caldas, Brazil
J. Cross[1], A. Haworth[1], P. C. Lichtner[2], A. B. MacKenzi[3], L. Moreno[4], I. Neretnieks[4], D. K. Nordstrom[5], D. Read[6], L. Romero[4], S. M. Sharland[1], C. J. Tweed[1]
[1]AERE, Harwell, UK
[2]University of Bern
[3]Scottish Universities Research & Reactor Centre (SURRC), Glasgow
[4]Royal Institute of Technology (KTH), Stockholm
[5]US Geological Survey, Menlo Park
[6]Atkins ES, Epsom, UK
December 1990

TR 90-22
Near-field high temperature transport: Evidence from the genesis of the Osamu Utsumi uranium mine analogue site, Poços de Caldas, Brazil
L. M. Cathles[1], M. E. Shea[2]
[1]University of Cornell, New York
[2]Battelle, Chicago
December 1990

TR 90-23
Geochemical modelling of water-rock interactions at the Osamu Utsumi mine and Morro do Ferro analogue sites, Poços de Caldas, Brazil
D. K. Nordstrom[1], I. Puigdomenech[2], R. H. McNutt[3]
[1]US Geological Survey, Menlo Park
[2]Studsvik Nuclear, Sweden
[3]McMaster University, Ontario, Canada
December 1990

TR 90-24
The Poços de Caldas Project: Summary and implications for radioactive waste management
N. A. Chapman[1], I. G. McKinley[2], M. E. Shea[3], J. A. T. Smellie[4]
[1]INTERRA/ECL, Leicestershire, UK
[2]NAGRA, Baden, Switzerland
[3]Battelle, Chicago
[4]Conterra AB, Uppsala

TR 90-25
Kinetics of UO_2(s) dissolution reducing conditions: numerical modelling
I. Puigdomenech[1], I. Casas[2], J. Bruno[3]
[1]Studsvik AB, Nyköping, Sweden
[2]Department of Chemical Engineering, E.T.S.E.I.B. (U.P.C.), Barcelona, Spain
[3]Department of Inorganic Chemistry, The Royal Institute of Technology, Stockholm, Sweden
May 1990

TR 90-26
The effect from the number of cells, pH and lanthanide concentration on the sorption of promethium on gramnegative bacterium (Shewanella Putrefaciens)
Karsten Pedersen[1], Yngve Albinsson[2]
[1]University of Göteborg, Department of General and Marine Microbiology, Gothenburg, Sweden
[2]Chalmers University of Technology, Department of Nuclear Chemistry, Gothenburg, Sweden
June 1990

TR 90-27
Isolation and characterization of humics from natural waters
B. Allard[1], I. Arsenie[1], H. Borén[1], J. Ephraim[1], G. Gårdhammar[2], C. Pettersson[1]
[1]Department of Water and Environmental Studies, Linköping University, Linköping, Sweden
[2]Department of Chemistry, Linköping University, Linköping, Sweden
May 1990

TR 90-28
Complex forming properties of natural organic acids. Part 2. Complexes with iron and calcium
James H. Ephraim[1], Andrew S. Mathuthu[2], Jacob A. Marinsky[3]
[1]Department of Water in Environment and Society, Linköping University, Linköping, Sweden
[2]Chemistry department, University of Zimbabwe, Harare, Zimbabwe
[3]Chemistry Department, State University of New York at Buffalo, Buffalo, NY, USA
July 1990

TR 90-29
Characterization of humic substances from deep groundwaters in granitic bedrock in Sweden
C. Pettersson, J. Ephraim, B. Allard, H. Borén
Department of Water and Environmental Studies, Linköping University, Linköping, Sweden
June 1990

TR 90-30
The earthquakes of the Baltic shield
Ragnar Slunga
Swedish National Defence Research Institute
June 1990

TR 90-31
Near-field performance of the advanced cold process canister
Lars Werme
Swedish Nuclear Fuel and Waste Management Co (SKB)
September 1990

TR 90-32
Radioclide transport paths in the nearfield – a KBS-3 concept study
Roland Pusch
Clay Technology AB and Lund University of Technology
July 1990

TR 90-33
PLAN 90
Costs for management of the radioactive waste from nuclear power production
Swedish Nuclear Fuel and Waste Management Co (SKB)
June 1990

TR 90-34
GEOTAB: User's guide – Version 1.8.2
Ergodata
October 1990

TR 90-35
Dose conversion factors for major nuclides within high level waste
Ulla Bergström, Sture Nordlinder
Studsvik Nuclear
November 1990

TR 90-36
Sensitivity analysis of groundwater flow Licentiate thesis
Yung-Bing Bao
Royal Institute of Technology, Department of Land and Water Resources, Stockholm, Sweden
December 1990

TR 90-37
The influence of fracture mineral/ groundwater interaction on the mobility of U, Th, REE and other trace elements
Ove Landström[1], Eva-Lena Tullborg[2]
[1]Studsvik AB, Nyköping
[2]SGAB, Gothenburg
December 1990

TR 90-38
Solute transport in fractured rock – Applications to radionuclide waste repositories
Ivars Neretnieks
Department of Chemical Engineering,
Royal Institute of Technology, Stockholm
December 1990

TR 90-39
Modelling of the movement of the redox front in the uranium mine in Poços de Caldas, Brazil
Leonardo Romero, Luis Moreno, Ivars Neretnieks
Royal Institute of Technology, Stockholm
June 1990

TR 90-40
Distinct element modelling of the rock mass response to glaciation at Finnsjön, central Sweden
Lars Rosengren[1], Ove Stephansson[2]
[1]Itasca Geomekanik AB, Falun, Sweden
[2]Division of Rock Mechanics, Luleå University of Technology, Luleå, Sweden
December 1990

TR 90-41
Ground water in crystalline bedrock
Kai Palmqvist
BERGAB-Berggeologiska Undersökningar AB
June 1990

TR 90-42
Development of clay characterization methods for use in repository design with application to a natural Ca bentonite clay containing a redox front
Ola Karnland, Roland Pusch
Clay Technology AB, Lund
December 1990